Airbursts and Cratering Impacts

2025 | Volume 3 | Pages: 1–26 | e-location ID: e20250001
DOI: 10.14293/ACI.2025.0001



Research Article

New Evidence of High-Temperature, High-Pressure Processes at the Site of the 1908 Tunguska Event: Implications for Impact and Airburst Phenomena

Gunther Kletetschka[1,2], Marian Takac[2], Lucie Smrcinova[2], Radana Kavkova[2], Dallas Abbott[3], Malcolm A. LeCompte[4], Christopher R. Moore[5,6], James P. Kennett[7], Victor Adedeji[8], Timothy Witwer[9], Kurt Langworthy[10], Joshua J. Razink[10], Valerie Brogden[10], Brian van Devener[11], Jesus Paulo Perez[11], Randy Polson[11], Teresa M. Eaton[12], Matthew J. Valente[13], David B. Lanning, Jr.[12], Yoav Rapoport[12], Argyro Reyes[12], Ravi Holladay[12], Michelle Madrigal[12], Aleksei Kiselev[14] and Allen West[9,*]

[1]Geophysical Institute, University of Alaska, Fairbanks, AK 99775, USA; [2]Faculty of Science, Charles University, Albertov 6, Prague 12843, Czech Republic; [3]Lamont Doherty Earth Observatory of Columbia University, Palisades, NY 10964, USA; [4]Elizabeth City State University, Center of Excellence in Remote Sensing Education and Research, Elizabeth City, NC 27909, USA; [5]South Carolina Institute of Archaeology and Anthropology, University of South Carolina, Columbia, SC 29208, USA; [6]SCDNR Heritage Trust Program, Land, Water, and Conservation Division, South Carolina Department of Natural Resources, Columbia, SC 27909, USA; [7]Department of Earth Science and Marine Science Institute, University of California Santa Barbara, Santa Barbara, CA 93106, USA; [8]Department of Natural Sciences, Elizabeth City State University, Elizabeth City, NC 27909, USA; [9]Comet Research Group, 2204 Lakewood Drive, Prescott, AZ 86301, USA; [10]CAMCOR, University of Oregon, 1443 E 13th Ave, Eugene, OR 97403, USA; [11]Electron Microscopy and Surface Analysis Lab, Nanofab, University of Utah, Salt Lake City, UT 84112, USA; [12]Biology and Chemistry Dept, College of Arts & Sciences, Embry-Riddle University, Prescott, AZ 86301, USA; [13]Life Sciences Department, Harford Community College, Bel Air, MD 21015, USA; [14]Minin Nizhny Novgorod State Pedagogical University, Nizhny Novgorod, Russia

*Correspondence to: Allen West, E-mail: CometResearchGroup@gmail.com

Received: 15 January 2025; Revised: 15 January 2025; Accepted: 23 January 2025; Published online: 8 February 2025

How to cite: Kletetschka G., et al. New Evidence of High-Temperature, High-Pressure Processes at the Site of the 1908 Tunguska Event: Implications for Impact and Airburst Phenomena. *Airbursts and Cratering Impacts*. 2025 | Volume 3 | Issue 1 | Pages: 1–26 | DOI: 10.14293/ACI.2025.0001

ABSTRACT

We report diverse shock-metamorphosed and melted grains from the 1908 airburst site in Russia, one of history's most significant and enigmatic cosmic events. Analysis of samples from a rimmed crater-like feature near the epicenter using scanning electron microscopy (SEM), transmission electron microscopy (TEM), electron backscatter diffraction (EBSD), and cathodoluminescence (CL) revealed evidence of extreme conditions. Our findings indicate heterogeneous shock pressures (~≥2 GPa) and temperatures (~≥1710°C) produced various microparticles, including FeO and aluminosilicate glass microspherules, melted quartz microspherules, carbon spherules, glass-like carbon, and melted minerals. Notably, quartz grains exhibit high-temperature melting and shock metamorphism, including planar deformation features (PDFs) and planar fractures (PFs), with some showing glass-lined internal fractures and melted silica coatings. Similarly, some feldspar grains display melted feldspar coatings. While multiple origins for these materials are possible – including an older crater and volcanism – the evidence best supports the 1908 Tunguska airburst hypothesis. The abundance of melted, shocked materials in the biomass-burning layer aligns with proposals that airburst fragments struck the Earth's

© 2025 The Author(s). This work has been published open access under Creative Commons Attribution License CC BY 4.0 https://creativecommons.org/licenses/by/4.0/, which permits unrestricted use, distribution and reproduction in any medium, provided the original work is properly cited. Conditions, terms of use and publishing policy can be found at www.scienceopen.com.

surface at velocities sufficient to produce shocked quartz. The coexistence of melted particles, shock-metamorphosed minerals, and unaltered grains suggests a heterogeneous energy distribution that created shallow craters and melted surface materials. These findings advance our understanding of airburst/impact mechanics, but few people have ever observed a dangerous airburst like Tunguska, so very little is known about them. Lacking sufficient real-world data, scientists should continue modeling these dangerous low-altitude airbursts to understand them better. The Tunguska event is a valuable case study demonstrating the urgent need to improve our planetary defense strategies.

KEYWORDS

Tunguska, airburst, shocked quartz, planar deformation features (PDFs), planar fractures (PFs), melted quartz, microspherules, hydrocode modeling

Introduction

The Tunguska event on the morning of June 30, 1908, stands as the most powerful cosmic impact in recorded history. Its enigmatic nature stems from the three puzzles: no visible impact crater despite the event's massive energy release [1], no recovered meteorite fragments [2], and the uncertainty about the impactor's composition – whether asteroid, comet, or another object [3–5]. These unresolved questions have spawned numerous competing theories and sustained scientific interest for over a century later [6, 7].

The explosion occurred over the Eastern Siberian Taiga, flattening 2,150 sq km of forest and generating seismic waves detected in England [3]. Scientists determined the epicenter by analyzing the radial pattern of fallen trees [8, 9] (Figure 1). The event released energy equivalent to 10-15 Mt of TNT [11, 12], yet left no obvious impact crater, suggesting the Tunguska object detonated as an airburst [1]. Figures 1 and 2 show the sampling site.

The Tunguska event demonstrates the destructive potential of near-Earth objects and has significant implications for planetary defense. Recent studies have identified similar high-energy airburst events at other sites, including the prehistoric village at Abu Hureyra in Syria [13–16] and the city at Tall el-Hammam in the Middle Bronze Age [17, 18]. Therefore, understanding the Tunguska event's mechanics is critical for historical reconstruction and future impact risk assessment.

Previous investigations of the Tunguska site have produced mixed results. Leonid Kulik's expeditions in the 1920s and 1930s documented extensive forest destruction but found no impact crater or significant meteorite fragments [8]. Later studies analyzed tree ring data to assess environmental impacts and date the explosion [19, 20], while soil analyses sought extraterrestrial materials from the bolide [21]. However, the soil materials previously attributed to the bolide are now understood to be products of post-impact acid rain rather than direct extraterrestrial input. Our study presents the first comprehensive evidence of airburst/impact proxies resulting from the Tunguska event.

Atmospheric modeling studies have estimated the impactor's size, composition, and trajectory [11, 12]. Artemieva and Shuvalov [6] expanded this research by comparing airbursts from Tunguska to Chelyabinsk, advancing our understanding of these phenomena. Longo's century-spanning review [22] documented the event's sustained scientific importance.

Recent studies have revealed new evidence about the Tunguska event. Kletetschka et al. [23] documented environmental impacts through magnetic, tree ring, and lake sediment analyses, all indicating a significant disturbance. Two potential impact craters have been proposed: Suzdalevo Lake in Central Siberia [24] and the 350-m-diameter Lake Cheko [7, 25], with local accounts suggesting Lake Cheko formed after the 1908 airburst.

Kletetschka's earlier work [26] identified magnetic anomalies in tree rings and rocks near the Tunguska site. While these findings suggested effects from the event, they represented indirect rather than direct impact evidence.

Tree ring studies [25, 27] documented the event's environmental effects, while a recent Farinella et al. [28] analysis clarified the physical processes involved, informing assessments of future impact risks.

Direct physical evidence of the extreme conditions generated by the Tunguska impact has remained elusive. While felled trees demonstrate the event's power, they reveal the temperatures and pressures at impact. Our study analyzes the event's subsurface samples collected from the epicenter during a 2008 centennial expedition (Figure 1). We identified microscopic particles and minerals showing evidence of extreme conditions, interpreted as airburst/impact proxies. Using advanced techniques, scanning electron microscopy (SEM), transmission electron microscopy (TEM), electron backscatter diffraction (EBSD), and cathodoluminescence (CL), we characterize these materials and their formation conditions. This microscopic evidence provided new insights into the event's immediate physical effects, complementing existing macroscopic data.

This study aims to:

1. Characterize Fe- and Si-rich microspherules, carbon spherules, melted and shocked minerals, and other impact-related particles from the Tunguska site.
2. Determine the formation temperatures and pressures of these materials.

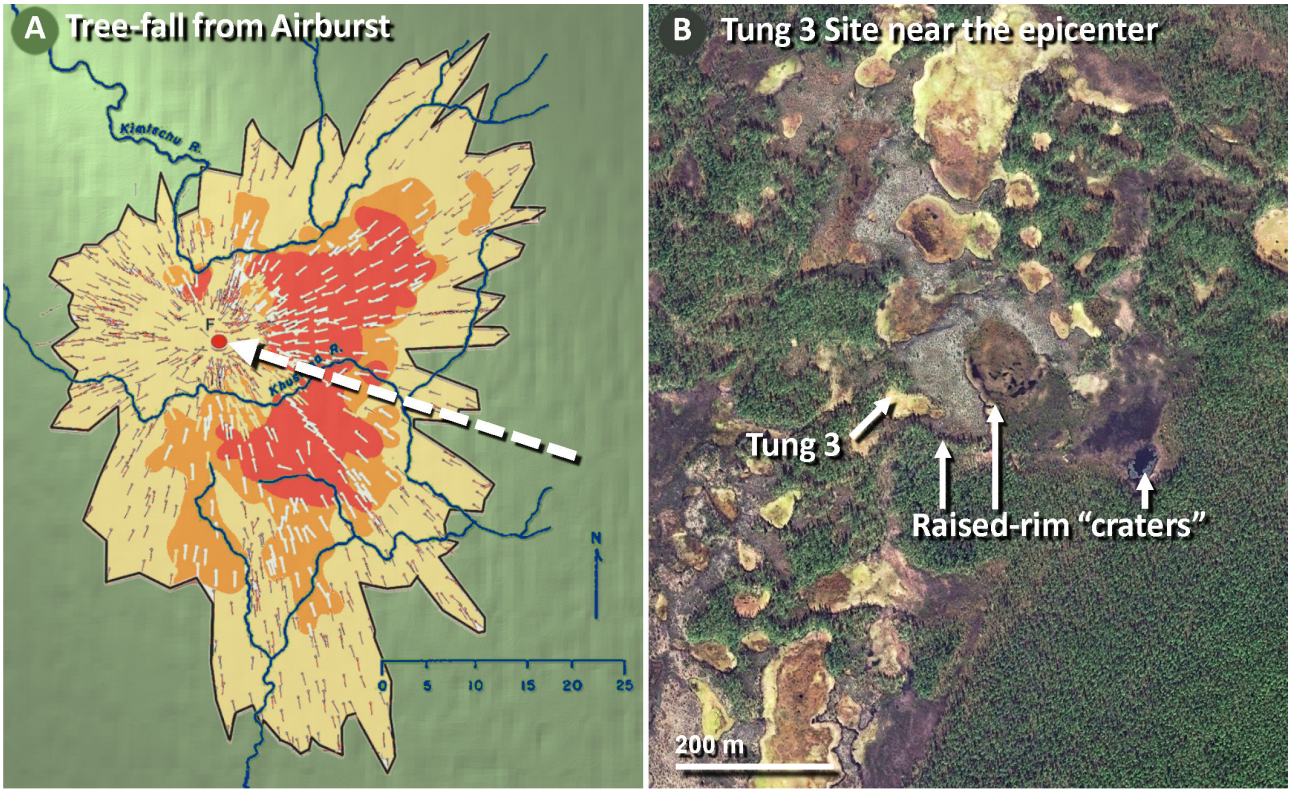


Figure 1: Location of sample site Tung 3 near the Tunguska epicenter. A) The airburst occurred over Siberia with an approximate entry angle shown as a dashed line. Our sampling site, Tung 3, is ~700 m northeast of the center of the red dot, the estimated location of the epicenter. The force of the aerial detonation felled tens of millions of trees in a "butterfly" pattern radiating away from the epicenter [7]. The pattern is ~75 km long by 60 km wide. Map adapted from Longo et al. [10]. B) The Satellite view of the Tunguska Tung 3 sampling site (60.90506°N, 101.95866°E) reveals numerous distinctive circular bog structures. We specifically selected the sampling site because it was on the raised rim of a crater-like feature. Image source: Google Earth, CNES/Airbus, Maxar Technologies. Map data acquired 5/2015, accessed 12/2024.

3. Identify formation mechanisms, including airburst effects, crater formation, plume dynamics, and secondary phenomena like lightning.
4. Develop a hydrocode model consistent with the observed evidence using a computer program that simulates the behavior of materials under short-duration temperature and pressure.
5. Evaluate implications for understanding airburst events and their ground-level effects.

This research advances our understanding of the Tunguska event while informing broader studies of impact cratering and airburst phenomena. Our findings help assess the hazards of near-Earth objects and interpret impact records across planetary bodies. The study also provides historical context for modern research on minor asteroid impacts and atmospheric entry processes.

Results and interpretations

Our analyses reveal shocked quartz grains with planar deformation features (PDFs) and planar fractures (PFs), glass-coated and glass-filled quartz grains, glass-coated feldspar grains, microspherules, melted titanomagnetite, and carbon spherules and glass-like carbon from biomass burning. Hydrocode modeling suggests that small bolide fragments may have created shallow surface craters. Results are primarily presented through captioned images consistent with the study's visual nature.

Shock-fractured and melted quartz

Previous studies near our sampling site documented shocked quartz with differing interpretations of its origin. Vannucchi et al. [29] attributed it to a volcanic gas eruption despite a lack of evidence that such events produce shock metamorphism. Hyanina [30] suggested an older impact crater source, although no other evidence supports this hypothesis. Our investigation confirms the presence of shock-metamorphosed and isotropized quartz grains in this area.

Our analyzed quartz grains show isotropic silica coating, glass-filled fractures, and glassy regions within the quartz matrix (Figures 3–13). Multiple analytical methods (SEM, TEM, CL, and EBSD) confirm these features as melted silica rather than cryptocrystalline or microcrystalline quartz. SEM-EDS reveals an oxygen/silicon ratio of ~39/61 wt% in partially melted grains, significantly lower than typical ratios for alpha quartz, agate, or chert (53/47 wt%) and hydrated



Figure 2: Sampling site. Location of Tung 3 site, as seen from the helicopter window. Note that the crater-like features with raised rims are generally assumed to be thermokarst features, though some researchers suggest they are impact craters.

silica (66/34 wt%). This oxygen depletion suggests that high-temperature melting caused partial SiO_2 dissociation, producing SiO_2 (~74 wt%) mixed with native Si (~26 wt%).

Analyses of quartz grains by electron backscatter diffraction (EBSD)

EBSD analysis of grain #07x12 shows lattice distortions, misorientations (1° to 5°), and Dauphiné twinning (Figure 4). The Local Orientation Spread (LOS) map indicates extensive grain damage. Dauphiné twins, rotated 60° around the c-axis, concentrate at boundaries between melted and unmelted regions of the monocrystalline quartz, suggesting their formation is directly related to melting.

Analyses of quartz grains by transmission electron microscopy (TEM)

TEM analysis of grain #07x12 reveals lamellae along specific crystalline planes (Figures 5 and 6), with both crystalline quartz and amorphous silica present (Figures 7 and 8). Selected area diffraction patterns display crystalline white spots with an amorphous silica halo.

Additional quartz grains show similar melting and shock features. Grain #24x-11 displays shock lamellae, a 39/61 wt% oxygen/silicon ratio, and lattice misorientation of up to 5° (Figure 13). Grain #17x-07b exhibits a 37/63 wt% oxygen/silicon ratio and glass-filled shock lamellae (Figure 14). CL imaging confirms melted silica and crystalline quartz in both grains.

A small fraction of sedimentary grains shows glass coatings and/or glass-filled planar deformation features or fractures. The glass composition typically matches the host minerals: quartz coatings on quartz grains, feldspar coatings on feldspar grains, and some grains occasionally displaying multi-element sediment coatings. This selective surface melting suggests an airburst/impact thermal pulse or high-temperature shockwave exposure.

Partially melted feldspar grains

Vesicular melted feldspar grains occur at low concentrations (80/kg) (Figures 14 and 15). These isotropic grains contain 11 wt% Na, 14 wt% Al, 38 wt% Si, and 37 wt% O, indicating oxygen depletion relative to stoichiometric albite.

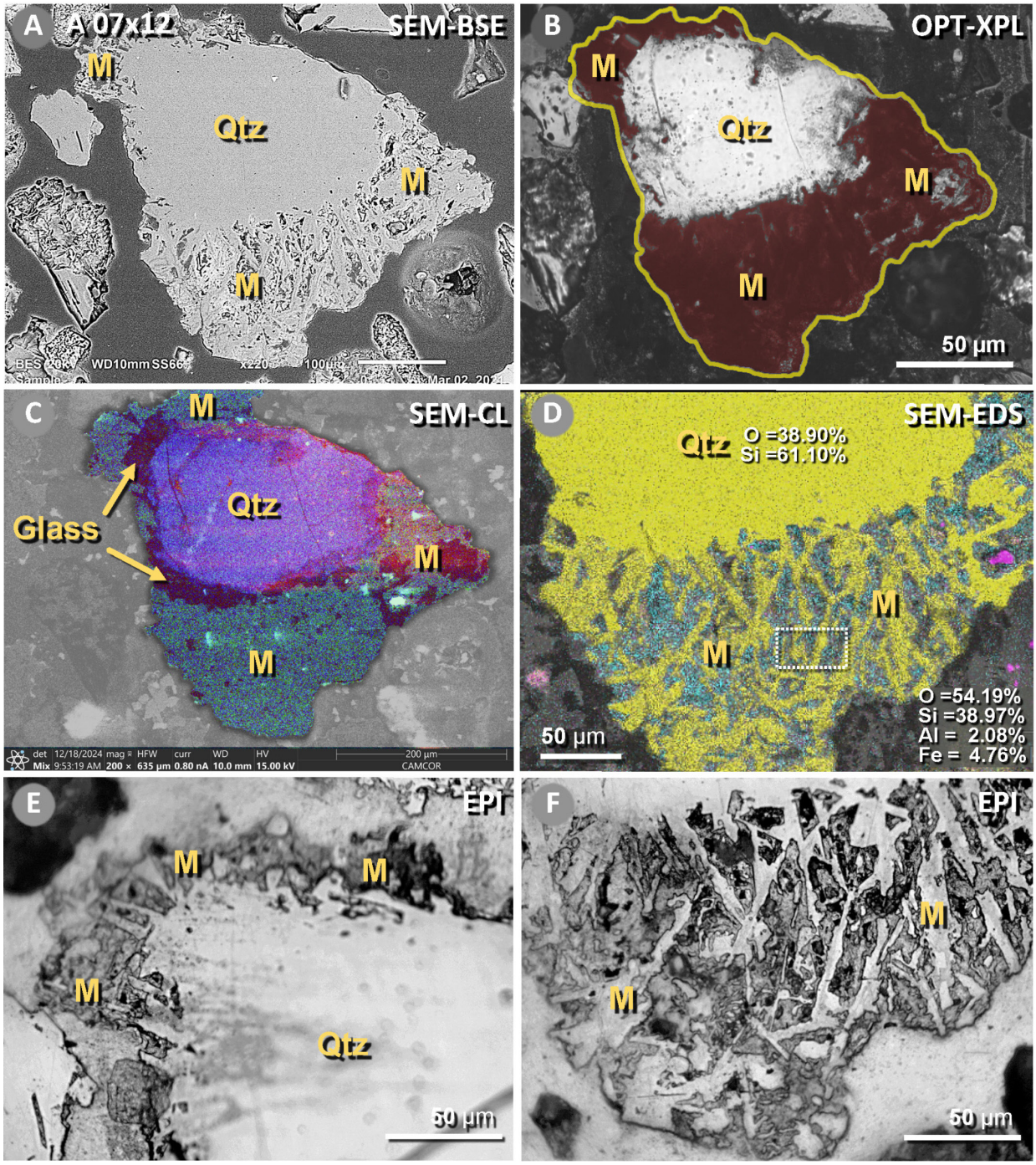


Figure 3: Optical, Scanning electron microscopy (SEM), and cathodoluminescence (SEM-CL) images. A partially melted, 500-µm-diameter quartz grain (#A 07x12). A) SEM-BSE image. "Qtz" indicates crystalline quartz, and "M" marks the amorphous dendritic area of the grain. A nearly identical dendritic grain was observed in impactites from Ries crater (Figure 8 from Trepmann et al. [31]) that they inferred to have crystallized directly from impact melt. B) An optical photomicrograph shows that the dendritic area (false-colored red) is isotropic under crossed polars (OPT-XPL), which is consistent with amorphous silica. C) SEM-CL image with a reddish-blue area (Qtz) indicating quartz that may have been heated and recrystallized but may also result from impurities in the quartz or damage by mechanical stress [32–35]. "M" marks dendritic areas of amorphous silica mixed with Al and Fe. Areas marked "Glass" are non-luminescent (black), indicating extensive lattice damage that melted the silica [32–35]. Contrast and brightness were decreased for the non-grain background to improve visibility. D) SEM-EDS elemental map reveals that the crystalline "Qtz" area has an oxygen/silicon ratio of ~39/61 wt%, much lower than quartz's typical stoichiometric values of 53/47 wt%. This low ratio is consistent with partial dissociation of the silica during melting, producing native Si mixed with SiO_2. This ratio eliminates the material as quartz cement or quartz overgrowth, composed of hydrated silica ($SiO_2 \cdot H_2O$) with an oxygen/silicon ratio of ~66/34 wt%. The dendritic area ("M") is composed of melted silica mixed with small concentrations of 4.76 wt% Fe and 2.08 wt% Al. E-F) Epi-illuminated photomicrographs show an amorphous dendritic area at panel A's upper left and lower left, respectively.

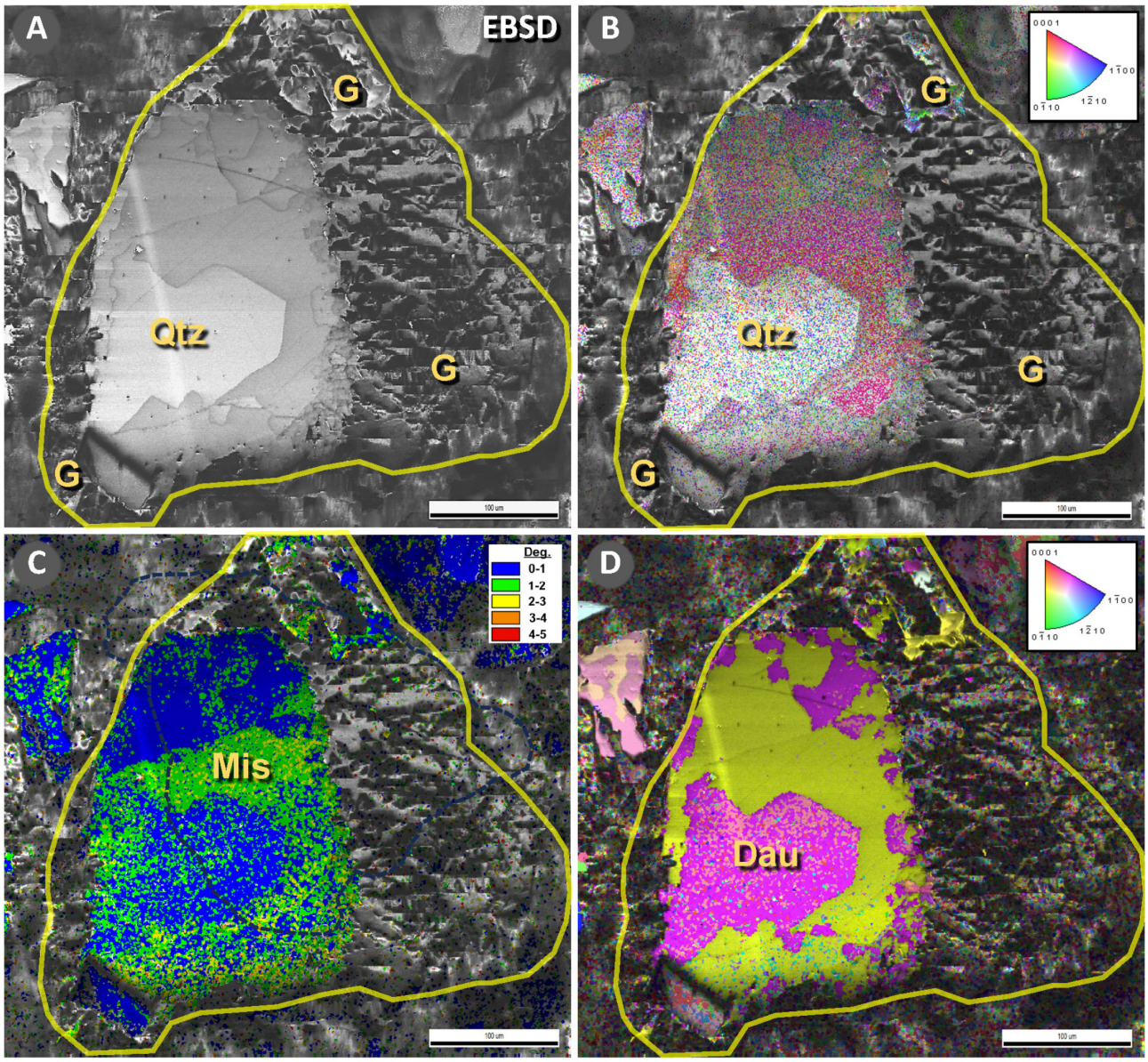


Figure 4: Electron backscatter diffraction (EBSD) of shock-fractured quartz grain (#07x12). This technique determines the crystalline structure and orientation of the crystal's planes at the quartz grain's surface. A) Image Quality (IQ) figure where "Qtz" indicates crystalline quartz and "G" represents glassy areas. B) Grain Reference Orientation Deviation (GROD) superimposed on IQ. Different colors represent crystalline lattice distortions into different crystalline planes, as indicated by the Miller-Bravais scale at the upper right. C) Local Orientation Spread (LOS) map superimposed on IQ reflects the degree of misorientation (0°-5°) of the crystal. The green-yellow-orange areas, marked "Mis," represent damaged crystalline lattice misoriented by 1° to 5°. D) Inverse Pole Figure (IPF) superimposed on IQ exhibiting quartz grain areas that have rotated 60° relative to the *c*-axis, so-called Dauphiné twinning ("Dau"). This feature can occur when a heated crystal melts and subsequently recrystallizes into a different orientation during cooling. Except for the largest area, Dauphine twinning in this grain is concentrated near the boundary between melted and unmelted areas, where it likely formed in response to higher ambient temperatures to which the grain was exposed.

Melted microspherules

Tunguska samples contain diverse microspherules. Fe-rich (200/kg), aluminosilicate glass (80/kg), and silica varieties. Fe-rich examples include a 55-µm diameter spherule (Figure 16A) and a 39-µm dendritic spherule (98.42 wt% Fe) (Figure 16D). Aluminosilicate specimens feature a sectioned 380-µm transparent spherule with large vesicles (Figure 16B). A 1.65-µm spherule with stoichiometric O/Si ratio was also identified (Figure 16C). Size, abundance, and composition match previous Tunguska findings [38, 39].

Partially melted minerals

A rare titanomagnetite grain ($Fe^{2+}(Fe^{3+}, Ti)_2O_4$) (40/kg), measuring 1950 µm, shows partial melting and intrusive aluminosilicate material, with Ti-Fe dissociation zones (Figure 17).

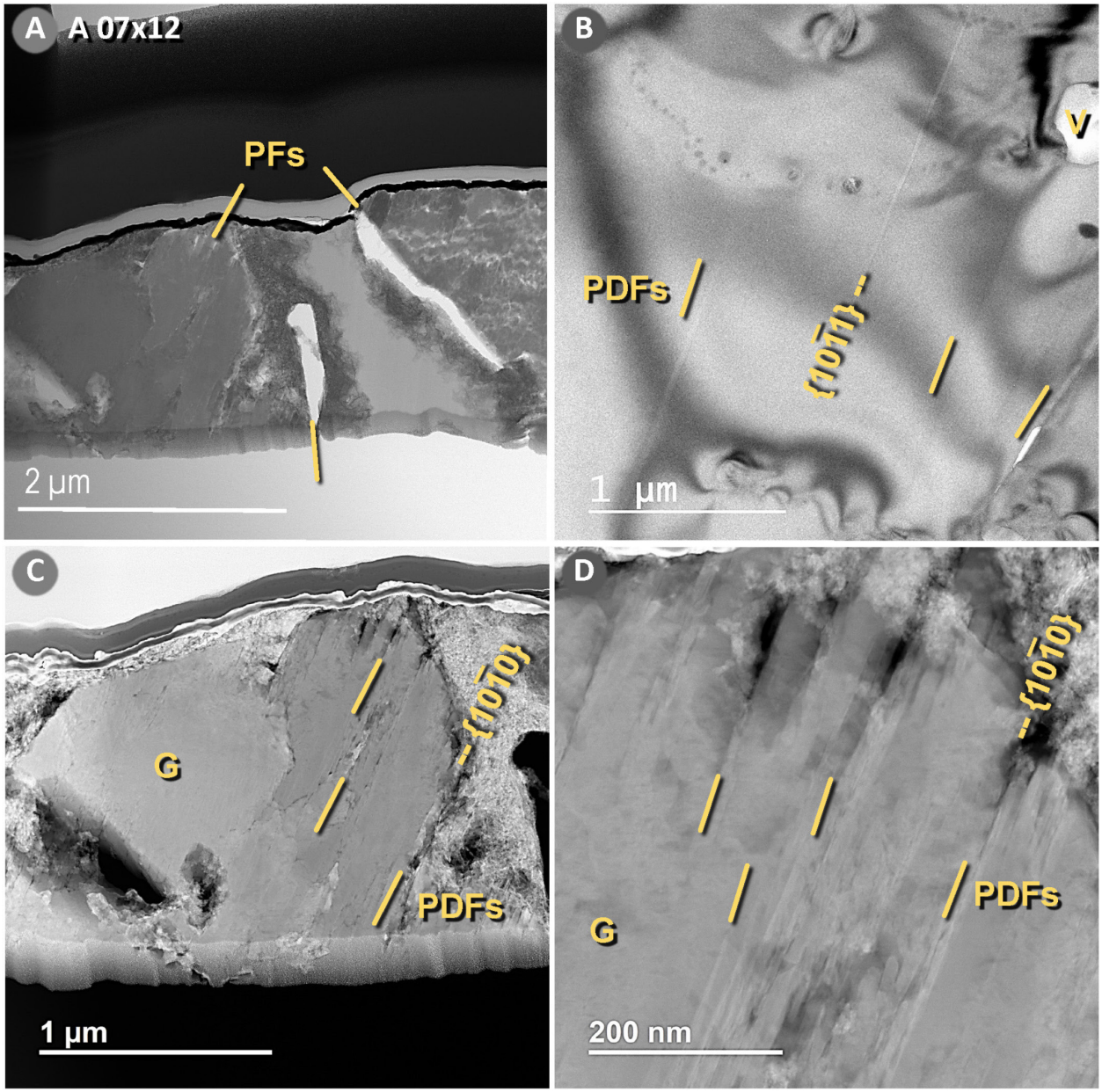


Figure 5: Transmission Electron Microscopy revealing shock-fracturing in a quartz grain (#07x12). All panels are HRTEM brightfield images. "PFs" identify planar fractures; "PDFs" mark planar deformation features; "G" marks areas of glass, as determined by SAD; and "V" marks vesicles. A) Low-resolution image of most of the FIB foil showing two large, glass-filled fractures. B), C), and D) High-resolution TEM images showing multiple lamellae (yellow lines) oriented to the $\{10\bar{1}0\}$ and $\{10\bar{1}1\}$ crystallographic planes of quartz, as determined by measurements with selected area diffraction (SAD).

Carbon spherules and glass-like carbon

Carbon particles (760/kg) include opaque black (13), oblong (4) oblong, and translucent/amber spherules (2) ranging from 60 to 700 µm in diameter (Figure 18A–B). Glass-like carbon fragments show vesicular structure and >98 wt% carbon content (Figure 18D–F).

Material types, characteristics, and the inferred temperatures and pressures associated with the Tunguska impact event are presented in Table 1.

Hydrocode modeling of the Tunguska airburst

Initial modeling used the Earth Impact Effects Program (EIEP) [41–43] (Table 2). Despite the program's limitations, it is commonly used for hydrocode simulations [42, 43, 45–50]. Based on studies by Pierazzo et al. [51] positively comparing Autodyn with other programs (iSALE, SOVA, SPH, CTH, ALE3D) and physical experiments, we applied EIEP results to Autodyn-2D analysis [52–64] (Figures 19 and 20). Input parameters are

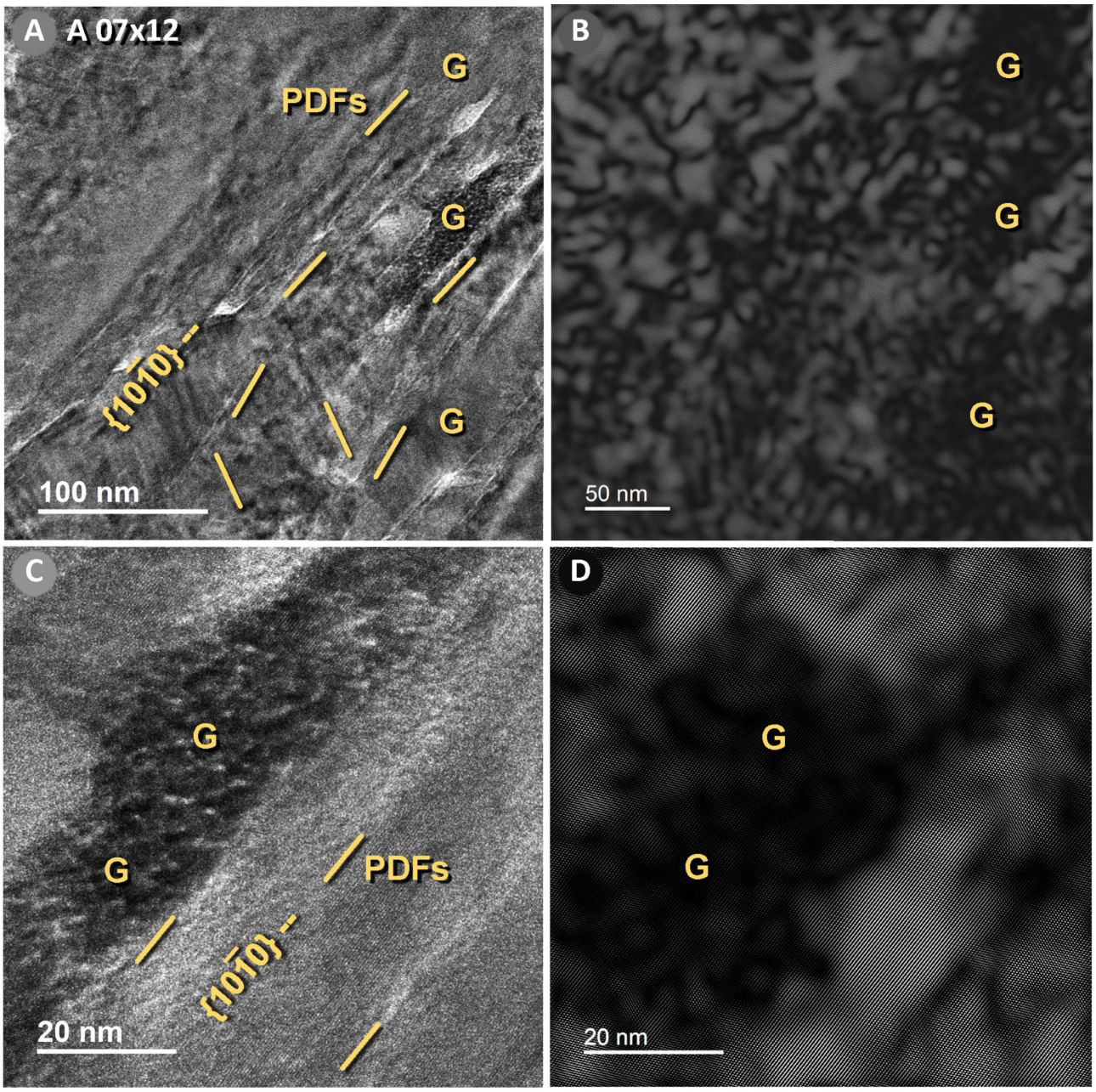


Figure 6: Transmission Electron Microscopy of shock-fractured quartz grain (#07x12). "PDFs" mark planar deformation features, and "G" marks areas of glass, as determined by SAD. A) and C) High-resolution TEM images of grain areas with mixed amorphous silica at "G," showing multiple lamellae (yellow lines) oriented to the $\{10\bar{1}0\}$ crystallographic plane of quartz (yellow lines), as determined by SAD. B) and D) Corresponding inverse fast Fourier transform (IFFT) images showing lighter-colored areas with crystalline lattice and darker-colored areas with amorphous or heavily damaged silica, marked as "G."

detailed in Supporting Information, https://zenodo.org/records/14727706.

Discussion

Tunguska surface sediment contains microspherules, melted minerals, and shocked quartz, indicating extreme temperatures and pressures. Multiple interpretations exist.

Prior impact event

Hryanina [30] reported shocked quartz in outcrops near our sampling site within an 8-km depression, suggesting an ancient impact crater. However, this interpretation was presented only in a conference abstract and lacks supporting evidence. Additionally, some melted grains show delicate, pristine features inconsistent with millions of years of preservation, suggesting recent formation.

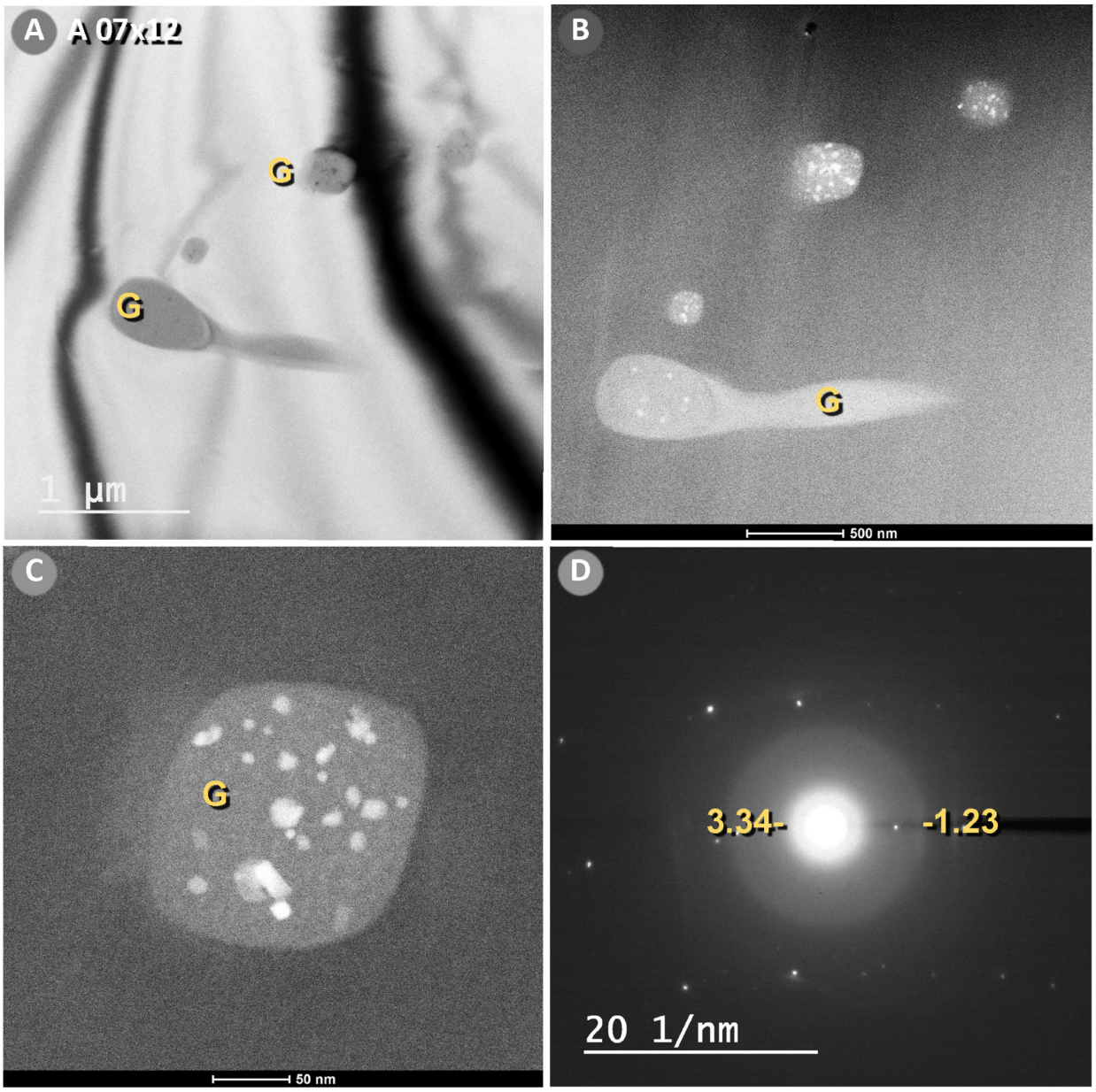


Figure 7: Transmission Electron Microscopy reveals amorphous areas of a quartz grain (#07x12). A-C) Dark-field images show inclusions mostly filled with amorphous silica (glass) and small crystallites. D) The selected area diffraction pattern is for inclusion in panel C. The small, white diffraction spots indicate crystallinity, while the diffuse halo suggests the presence of amorphous silica with characteristic d-spacings of 3.34 and 1.23.

Volcanism

Vannucchi et al. [29] attributed shocked quartz near our sampling site to hyperexplosive volcanic gas eruption. However, volcanic pressures are orders of magnitude below those needed for shocked quartz formation [66–68], and magma temperatures cannot achieve the melting of quartz grains (≥1713°C).

Tectonic deformation

While fault motion can create deformation lamellae and macro-scale melting [69, 70], tectonic processes cannot produce PDFs, glass-coated quartz, or silica-filled fractures in individual quartz grains.

Lightning

Lightning strikes can produce microspherules, meltglass, vesiculated minerals [71], and potentially shock-metamorphic features in rocks [72–74], although the latter is disputed [75]. Lightning also occurs frequently during volcanic eruptions [76]. However, lightning generated during the Tunguska airburst would have differed significantly from typical thunderstorm or volcanic lightning.

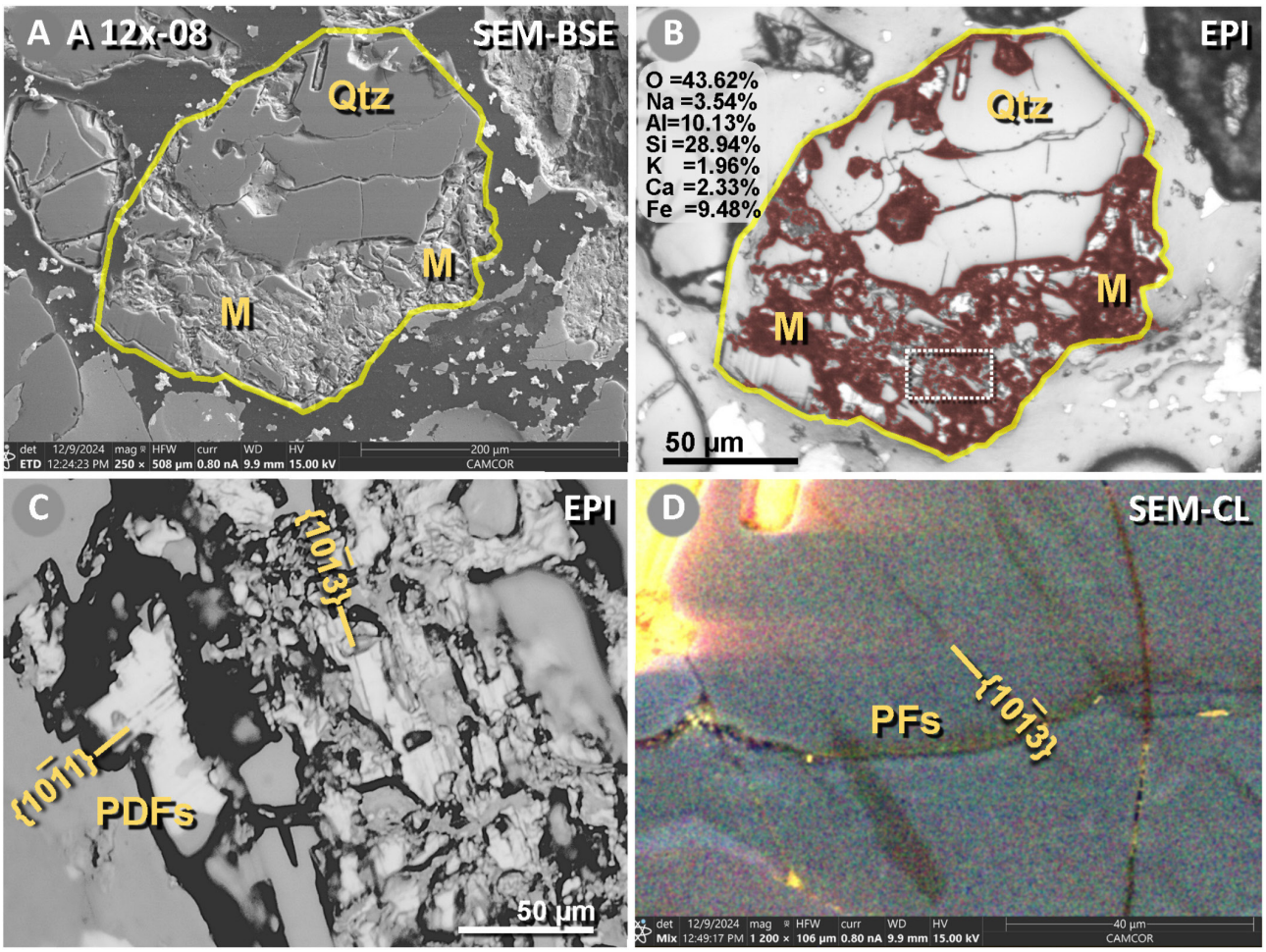


Figure 8: Shocked quartz grain: optical, scanning electron microscopy (SEM), and cathodoluminescence (SEM-CL) images (grain #A 12x-08). "PFs" identify planar fractures; "PDFs" mark planar deformation features, and "G" marks areas of glass, as determined by SAD. A) SEM-BSE image and B) epi-illuminated image (EPI) of ~330-µm-diameter quartz grain (#A 12x-08). "M" marks a dendritic area indicative of melted silica. C) EPI image showing planar deformation features (PDFs) oriented to the {10$\bar{1}$1} and {10$\bar{1}$3} planes and spaced ~1-2 µm apart. D) The SEM-CL image with a bluish matrix indicates crystalline quartz. Non-luminescent (black) bands indicate melted silica along planar and sub-planar lamellae [32–35].

In airburst-generated lightning, charge separation occurs through debris particles rather than water droplets or ice crystals. The dust/debris cloud produced by the airburst would have distinct electrical conductivity properties due to its unique composition and the extreme temperatures involved. These high temperatures would enhance ionization processes, while the strong shock waves could influence plasma formation.

Additionally, the particle size distribution and composition of airburst debris differ substantially from storm clouds, potentially affecting the intensity and character of the resulting electrical discharges. These differences suggest that while lightning may have contributed to the formation of some features in our samples, the mechanism would have been fundamentally different from typical terrestrial lightning processes. In any event, this type of lighting is airburst-related.

Forest fires

Forest fires cannot achieve temperatures sufficient for quartz melting at ≥1713°C) [40, 77, 78], making them an inadequate explanation for the observed evidence. Furthermore, Abramov et al. [79] documented that the Tunguska fire ignited simultaneously across >2000 km^2, unlike typical fire progression. Florenskiy's [39] firsthand observations revealed distinctive characteristics inconsistent with normal wildfire behavior: the event produced only a "treetop fire" that scorched the upper surfaces of trees while leaving living tree trunks largely intact. The selective burning of conifer needles and small twigs, combined with the survival of some trees near the epicenter despite millions being toppled at greater distances, suggests a brief, high-altitude thermal pulse rather than a conventional forest fire. These observations indicate a transient event, incapable of quartz and feldspar melting, contradicting a forest fire or the airburst's

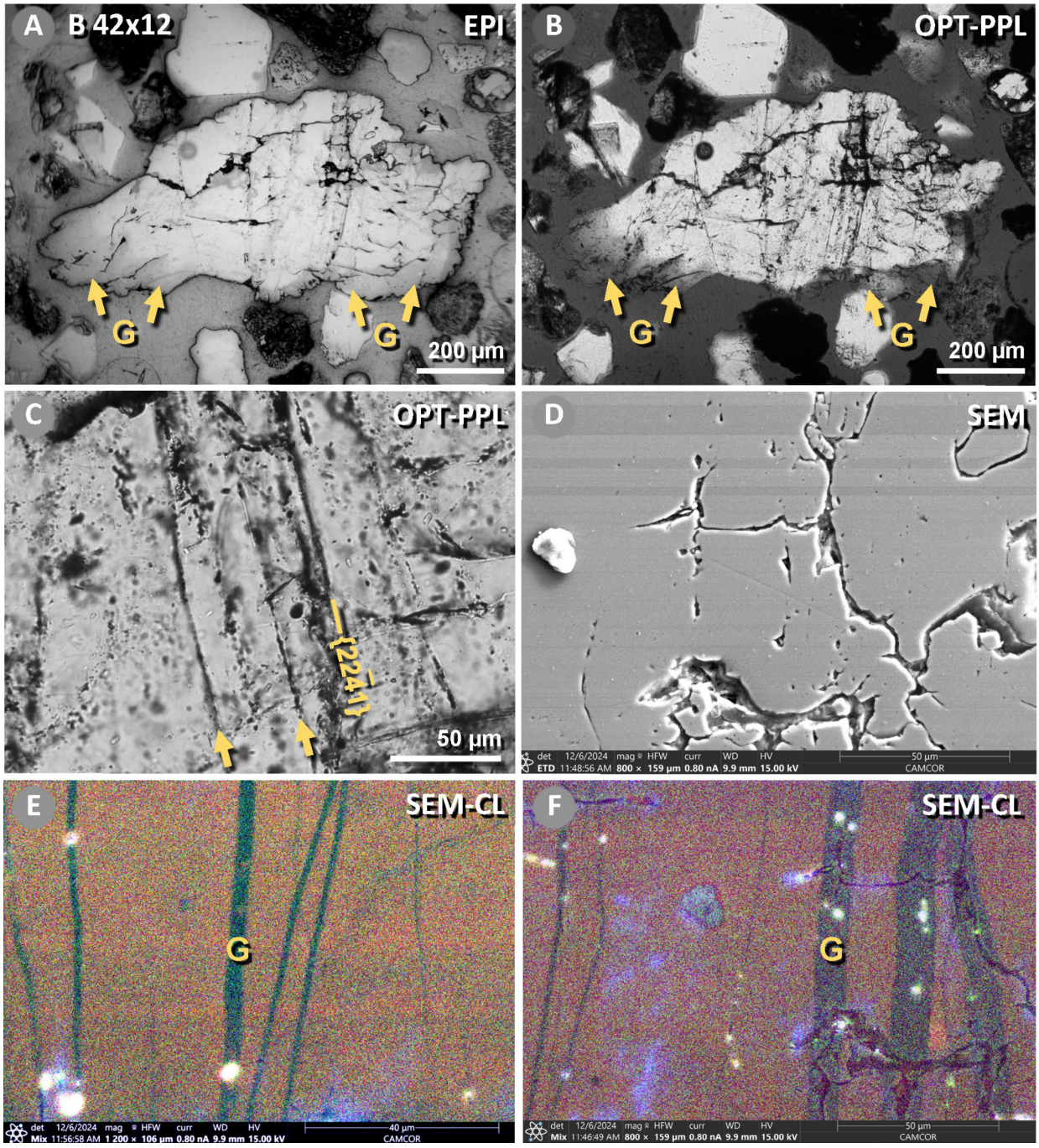


Figure 9: Optical, Scanning electron microscopy (SEM), and cathodoluminescence (SEM-CL) images. Grain #42x12. A) Epi-illuminated optical image and B) optical plane-polarized image (OPT-PPL) of ~1030-µm-diameter quartz grain. B) "G" marks darker gray areas indicative of melted silica that is isotropic under crossed polars. C) OPT-PPL image showing planar fractures (PFs) oriented to the $\{22\bar{4}1\}$ plane. D) SEM image of glass-filled fractures. E-F) SEM-CL images with reddish indicating crystalline quartz. "G" marks non-luminescent areas (black), indicating fully melted silica along sub-planar lamellae.

thermal pulse as primary mechanisms for the observed mineralogical changes.

Quartz overgrowth

SEM-EDS analyses rule out hydrated silica overgrowth as an explanation for the glass-coated and glass-filled quartz grains. Standard quartz overgrowth exhibits Si/O ratios of approximately 66/34 wt%, whereas the observed quartz coatings show distinctly different ratios of approximately 39/61 wt%. Additionally, microscopic examination reveals that these grains lack the crystalline structure characteristic of crypto- or micro-crystalline quartz, which typically

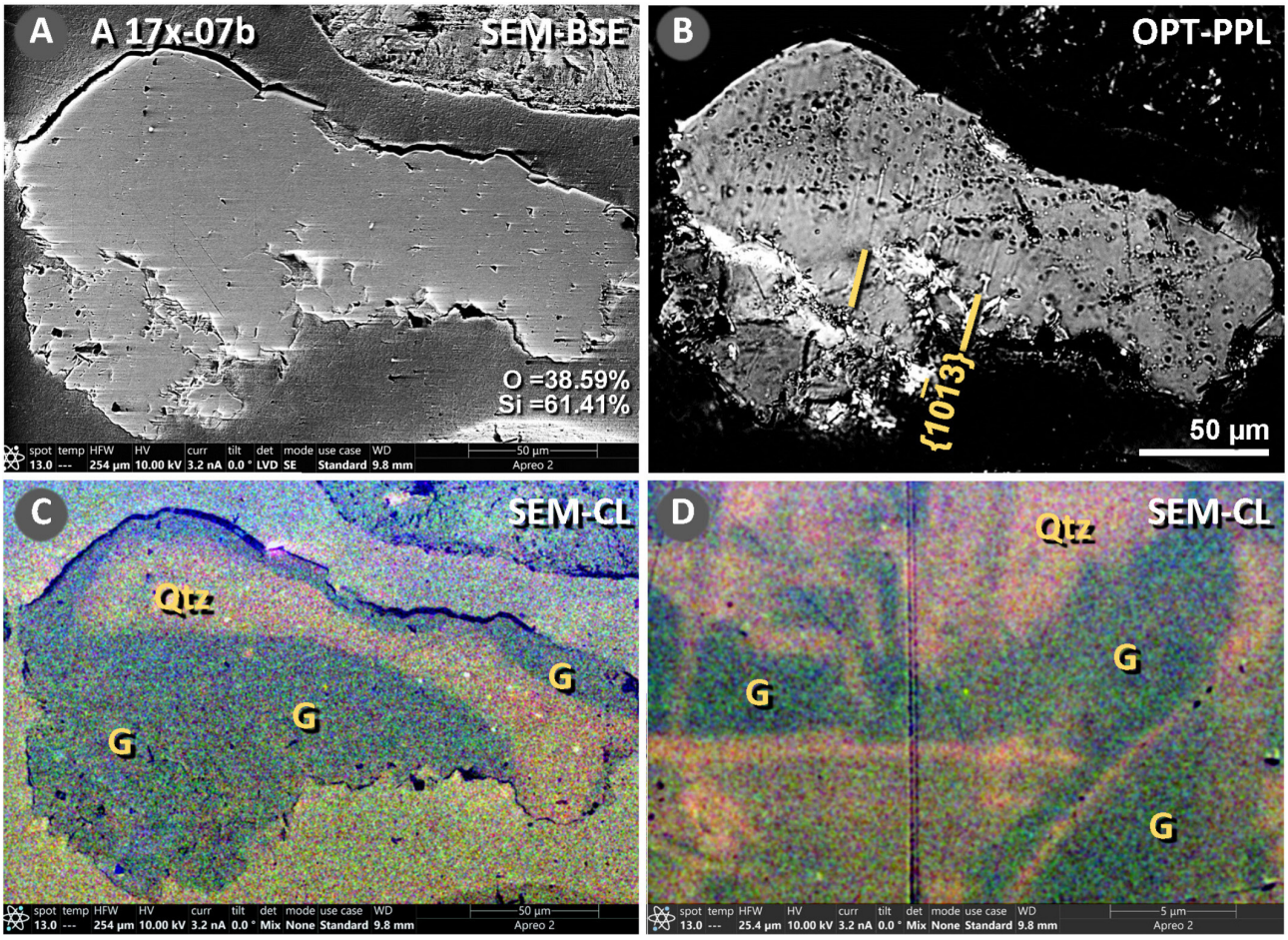


Figure 10: Optical, SEM, EBSD, and CL images of grain (#17x-07b). A) SEM-BSE image of a grain with an oxygen/silicon ratio of ~39/61 wt%, lower than quartz's typical stoichiometric values of 53/47 wt%, consistent with partial dissociation of the silica during melting. B) OPT-PPL image showing selected glass-filled PDFs (yellow lines) oriented to the {10$\bar{1}$3} plane. C-D) SEM-CL images reveal the crystallinity of the quartz grain. Dark areas ("G") indicate melted silica (non-crystalline quartz), and the orange areas ("Qtz") represent areas that appear to have melted and recrystallized.

displays detectable crystallites under both SEM and optical microscopy.

Tunguska airburst event

The Tunguska airburst shockwave, while devastating, lacked sufficient pressure to generate shocked quartz [52, 80]. Alternatively, although shocked quartz can be produced during impact cratering, the origin of crater-like features in the Tunguska area, including those at our sampling site, remains debated. Florenskiy [39] attributed these depressions to thermokarst activity (ground subsidence from permafrost melting) rather than impact processes.

However, several researchers have proposed that fragments from the disintegrating body did reach the Earth's surface, creating small impact features [2, 7, 81–83]. The most prominent example is Lake Cheko, a 350-m-diameter depression that Gasperini et al. [7] and Fantucci et al. [25] suggest may be an impact crater, supported by local accounts claiming the lake's absence before 1908. This interpretation of Lake Cheko remains controversial, highlighting the broader uncertainty surrounding the formation of crater-like features in the Tunguska region

Fragmentation during cosmic body airburst appears to be the norm, regardless of altitude, suggesting the Tunguska bolide likely fragmented as well. Multiple well-documented airburst events support this conclusion. The 2013 Chelyabinsk airburst occurred at 29.7 km altitude [6, 84–87], producing numerous meteorite fragments, including two massive pieces weighing 64.7 and 540 kg [88]. The latter fragment created a 9-m-wide crater in a frozen lake [85]. Similarly, the Tagish Lake meteorite's airburst in January 2000 occurred ~29 km above British Columbia, Canada, creating an elliptical strewn field measuring 5×16 km that contained over 10,000 fragments up to ~2.3 kg [89, 90]. The Campo del Cielo meteorite field in Argentina provides another example, where multiple fragments created shock-generated craters up to 26.5 m in diameter and 6 m deep in unconsolidated surface sediments. Thus, it is

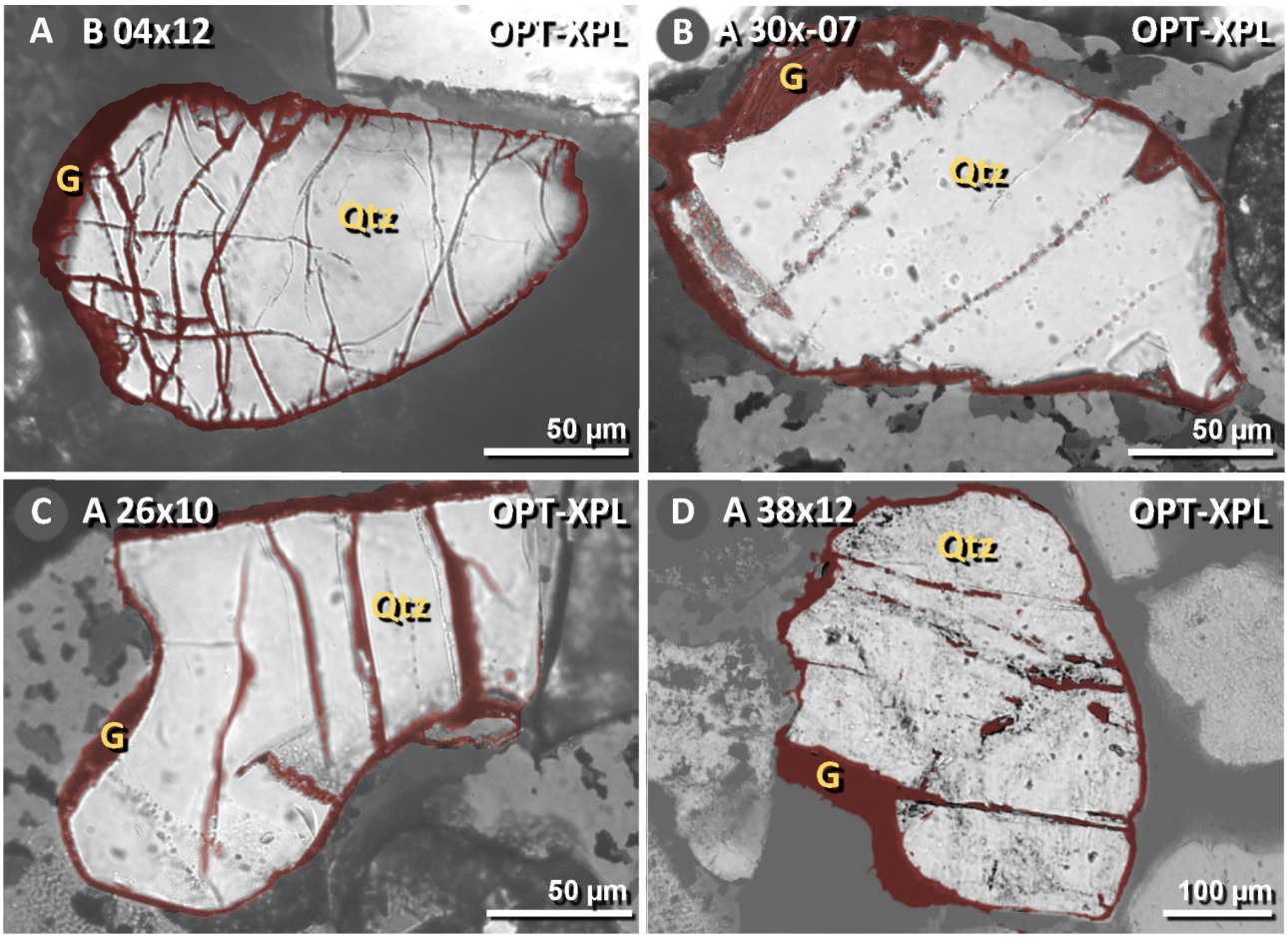


Figure 11: Optical images of meltglass-coated, glass-filled quartz grains. A-D) Portions of the isotropic grains under crossed polars are marked in false-colored red ("G") and subsequently identified as melted quartz using CL, TEM, and/or EBSD. "Qtz" denotes areas of crystalline quartz. To improve visibility, contrast and brightness were decreased for the non-grain backgrounds.

likely that fragments from the Tunguska airburst struck Earth's surface.

While no definitive Tunguska bolide fragments have been recovered, preservation conditions may explain this absence. Unlike meteorites in desert regions, which preserve well [91–93], those in environments with higher moisture and freeze-thaw cycles – conditions present at Tunguska – typically degrade rapidly [92]. In addition, if the fragments hit the Earth at ~2 km/s, they would have broken into tiny, hard-to-find pieces.

Hydrocode modeling demonstrates that the Tunguska event likely produced conditions sufficient for shock metamorphism. The model indicates shockwave velocities exceeding 2 km/s, temperatures above 4000 K lasting several seconds, and fragment impact pressures greater than 2 GPa. These conditions, though brief, could generate shock metamorphism, melt sedimentary grain surfaces, and force melted silica into fractures through jetting [94–96]. When standard Tunguska airburst parameters are entered into the Earth Impact Effects Program (developed by impact scientists Marcus, Melosh, and Collins [41, 43, 44]), the model predicts that "*large fragments may strike the surface*" (Table 2). This modeling supports the possibility that impacting fragments created small craters, consistent with the raised-rim feature from which we collected our samples.

Anomalous evidence

FeO and aluminosilicate glass microspherules present in our samples indicate temperatures reached 1300-1400°C [77, 97]. Even more significantly, we discovered melted quartz microspherules, which require temperatures above 1710°C, quartz melting point [98]. Such extreme temperatures align with those documented in known airburst and impact events [6, 11, 12], providing evidence for similar processes at Tunguska.

The observed partial melting of quartz and feldspar, along with filled fractures, likely resulted from intense thermal radiation during the airburst. Historical accounts from the 1908 Tunguska event provide supporting evidence - witnesses in Vanavara village, approximately 60 km from the epicenter, reported severe thermal burns. If the thermal radiation was sufficient to cause human burns at that distance,

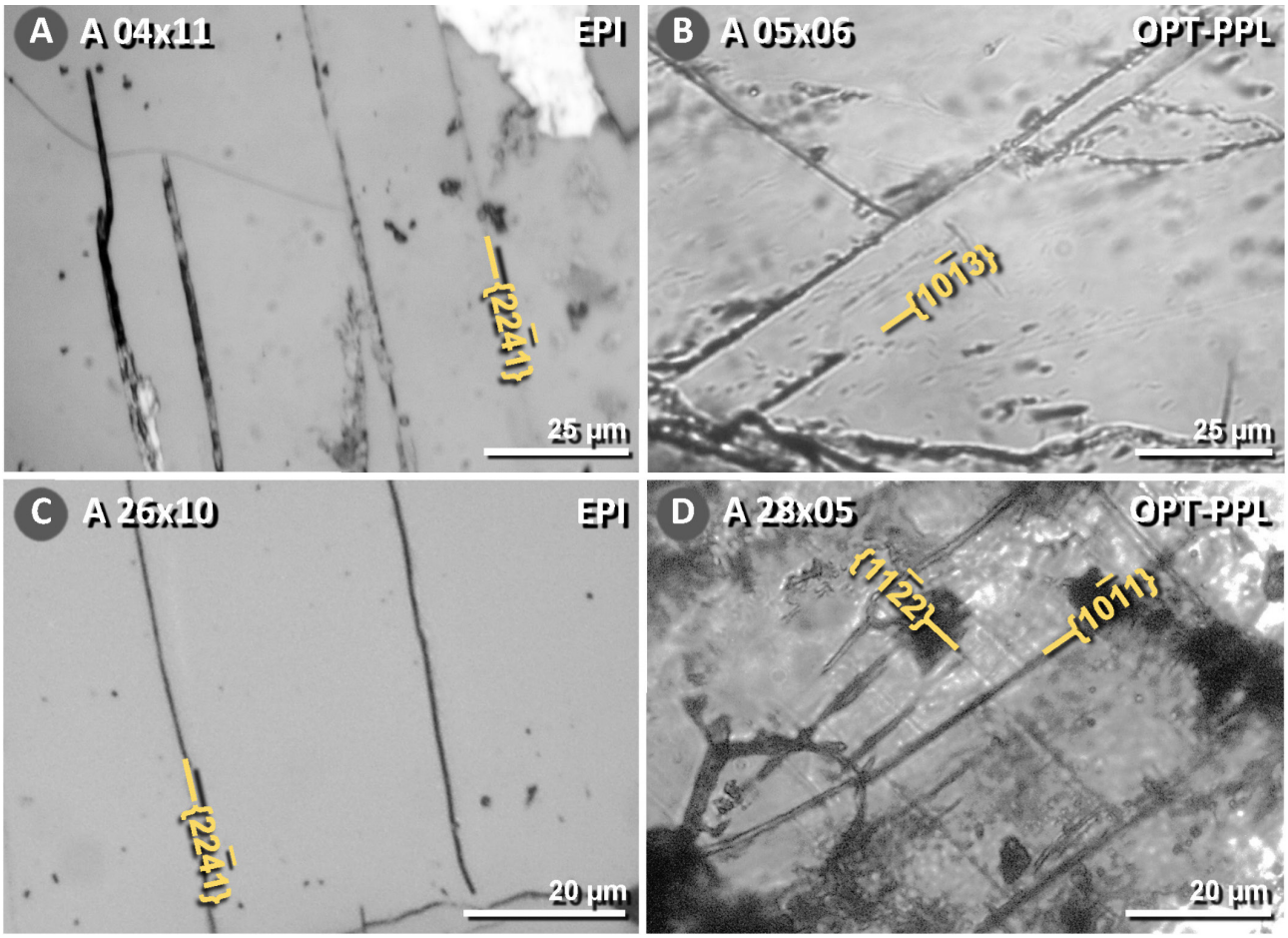


Figure 12: Quartz grains displaying planar fractures (PFs). A-D) Epi-illuminated and plane-polarized optical images of glass-filled planar fractures (PFs) in selected quartz grains. Figures 5, 6, 8, and 9 also display PDFs and PFs.

areas closer to the epicenter would have experienced temperatures well above the melting points of quartz (~1670°C) and feldspar (~1200°C). The brief but extreme heat pulse could explain the observed partial melting patterns, while rapid cooling would account for the fracture-filling features.

The samples' carbon spherules and glass-like carbon structures indicate rapid heating and cooling of organic material, primarily wood, tree sap, and vegetation [78, 99]. These particles form at temperatures between 800° and 1500°C [100], supporting evidence for intense heat generation during the Tunguska event. The presence aligns with documented widespread forest fires following the 1908 explosion [2, 39, 79].

The discovery of partially melted minerals provides further evidence of extreme temperatures. Some quartz grains display evidence of surface melting, indicative of temperatures ≥1710°C. Titanomagnetite grains showing partial melting indicate temperatures reached approximately 1625°C [101]. Feldspar grains exhibit oxygen depletion, suggesting partial dissociation during rapid heating [102, 103], another characteristic of brief, high-temperature events.

EBSD analysis reveals lattice distortions and misorientations in quartz grains [104], quantifying the strain they experienced. The observed misorientations of up to 5° indicate moderate shock pressures of 2-10 GPa [105–107]. While these pressures are below those typical of crater-forming impacts, they match shock wave pressures documented in large airburst events [17, 18, 43, 52, 108].

Shock-fractured quartz grains provide evidence of high-pressure conditions. The identified planar deformation features (PDFs) and planar fractures (PFs) are characteristic shock metamorphic indicators [37, 109]. While typically associated with crater-forming impacts, these features can also result from powerful airburst-generated shock waves [45, 110]. This possibility suggests that even small Tunguska bolide fragments striking Earth's surface at sufficient velocity could have produced the shocked quartz and melted sedimentary grains found in our samples.

Individual quartz grains display both crystalline and amorphous regions, with evidence of recrystallization, indicating shock melting followed by rapid cooling [111]. Oxygen depletion in quartz grains suggests partial dissociation at

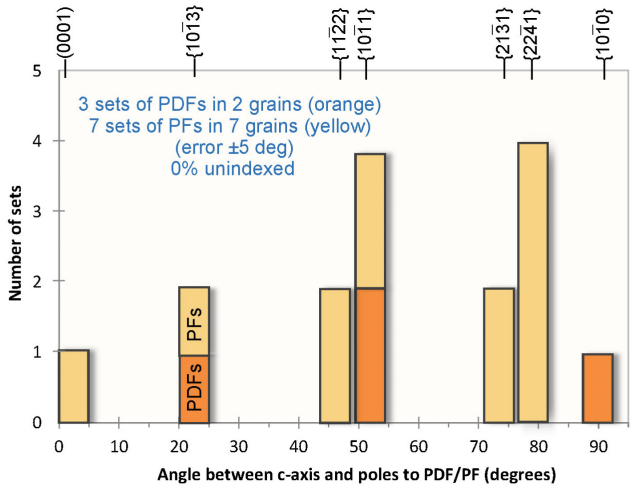


Figure 13: Crystallographic indexing of shock lamellae. After using optical microscopy to identify shocked quartz candidates (10 grains in 25 g = 400/kg, or 10 in ~4,000 quartz grains), we investigated further using the universal stage. U-stage indexing was problematic because some grains had been thermally distorted; however, lamellae in other areas were planar and parallel and could be indexed. The crystallographic axes were plotted with the ANIE indexing program [36]. All observed lamellae are among those commonly reported in shocked quartz studies [37]. The small sediment sample sizes (25 g) limited the scope of the investigation, so the observed distribution of lamellae may not be statistically representative.

high temperatures and subsequent rapid quenching [112]. The presence of Dauphiné twins further supports rapid thermal stress conditions [113].

Similar proposed airburst/impact events

As West et al. [52] discussed, impact researchers have identified at least eight touch-down airbursts within the last ~11,700 years across Western Europe (2.2 million km^2). Most are estimated to have been much larger than Tunguska but display the same evidence: microspherules, shocked quartz, melted minerals, and potential cratering. These sites include the Chrudim/Pardubice region in the Czech Republic [114] and a series of related strewn fields across the Czech territory [115]. In Germany, multiple impact sites have been documented: the Saarlouis structure with distinctive black glass melt rocks [116], the Chiemgau field showing evidence of a Holocene impact with archaeological connections [117–119], the Middle-Pleistocene Niederrhein deposit [120], the Holocene Franconia crater field [121], and the Pleistocene/Holocene Sachsendorf Bay structure [122]. Additionally, a 6400-year-old strewn field has been identified in Finland [123].

This distribution suggests a touch-down airburst recurrence rate of approximately one event per 1500 years across Western Europe. However, this estimate carries significant uncertainties due to limited data on touch-down airbursts. While more research is needed to determine an accurate recurrence rate, these findings indicate a meaningful threat from future airbursts, particularly over densely populated areas.

Implications for planetary defense

In 2023, a 30-60 m asteroid (2023 NT1) passed within only about one-quarter of the Earth-Moon distance – it was only discovered two days after it had passed Earth [52, 124, 125]. It had a potential impact energy of 10 Mt [124, 125], approximately similar to the Tunguska event. If this asteroid had exploded over a major city, it could have produced much greater damage than at Tunguska in a remote area of Siberia. This event is a reminder of the magnitude of the threat posed by small, difficult-to-detect bolides that produce highly destructive touch-down airbursts [52].

The Tunguska airburst is significant because it was the first example in modern times demonstrating that a relatively small asteroid or comet fragment can result in massive surface damage. Because only a few people have ever observed a dangerous airburst, such as Tunguska and Chelyabinsk, very little is known about them. Without sufficient real-world data, scientists must continue modeling these low-altitude airbursts to better understand the physics and effects of thermal radiation, shockwave propagation, and small crater formation. This study provides evidence and modeling suggesting that small bolide fragments ejected from the airburst can strike the Earth's surface with high energy at high velocities.

The evidence from Tunguska highlights the need for robust detection and mitigation strategies before a future disastrous airburst occurs over a populated area. This potential threat is especially serious because modern detection efforts primarily focus on larger bolides with limited capability of detecting smaller ones. Detecting smaller Earth-crossing bolides would require an array of space-based infrared telescopes and ground-based observatories capable of detecting these dangerous objects well before their arrival. Furthermore, it is necessary to develop adequate methods to deflect or disrupt these incoming bolides, but such telescopes and mitigation strategies are currently inadequate and expensive. Thus, the Tunguska event is a valuable case study demonstrating the urgent need to improve our planetary defense strategies.

Conclusions

Multiple analytical techniques provide evidence of extreme conditions during the 1908 Tunguska event, challenging previous assumptions about this cosmic airburst. The findings reveal a complex, heterogeneous field of high temperatures and pressures, with local temperatures exceeding 1710°C and shock pressures above 2 GPa, likely caused by bolide fragments striking the Earth's surface after the airburst. Multiple lines of evidence support these extreme conditions, including FeO and aluminosilicate glass microspherules, melted quartz microspherules, carbon spherules, and glass-like carbon structures. The presence of partially melted minerals and shock-fractured quartz grains with characteristic shock metamorphic features further corroborates the intense conditions present during the event.

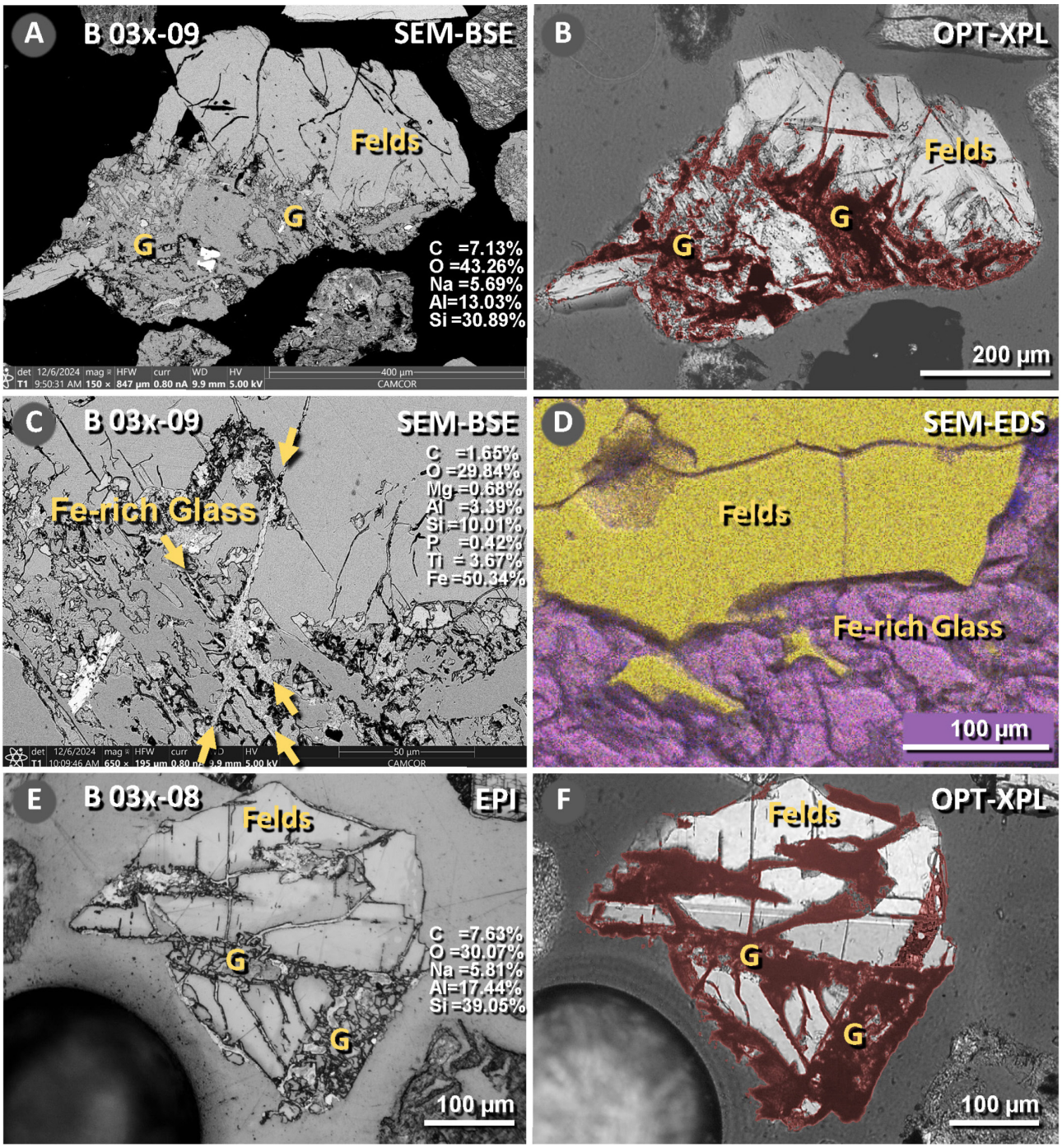


Figure 14: **Partially melted feldspar grains.** A) SEM-BSE image of sodic feldspar (albite) grain (#B 03x-09), as indicated by SEM-EDS. B) Optical image under crossed polars (OPT-XPL) shows that grayscale portions of the grain are anisotropic ("Felds"), whereas the false-colored red areas are isotropic ("G"), indicating parts of the grain were melted. C) Close-up SEM-BSE image of the grain in panel A, showing that some feldspar lamellae containing intrusive material, dominated by Fe, Ti, and Si, as determined by SEM-EDS. Crossed polars show the intrusive areas to be isotropic. D) SEM-EDS elemental map a portion of grain in panel A. The yellow area is crystalline feldspar, and the reddish area is Fe-Ti-Si glass. E) SEM-BSE image of another sodic feldspar grain (#B 03x-08), as indicated by SEM-EDS. F) Optical image under crossed polars shows that portions of the grain are anisotropic ("Felds"), whereas the false-colored red areas are isotropic ("G"), indicating parts of the grain were melted.

The coexistence of melted particles, shock-metamorphosed minerals, and unaltered grains points to a heterogeneous energy distribution characteristic of airburst events. These findings enhance our understanding of airburst mechanics and their ground-level damage potential while contributing valuable data to the broader study of impact cratering and

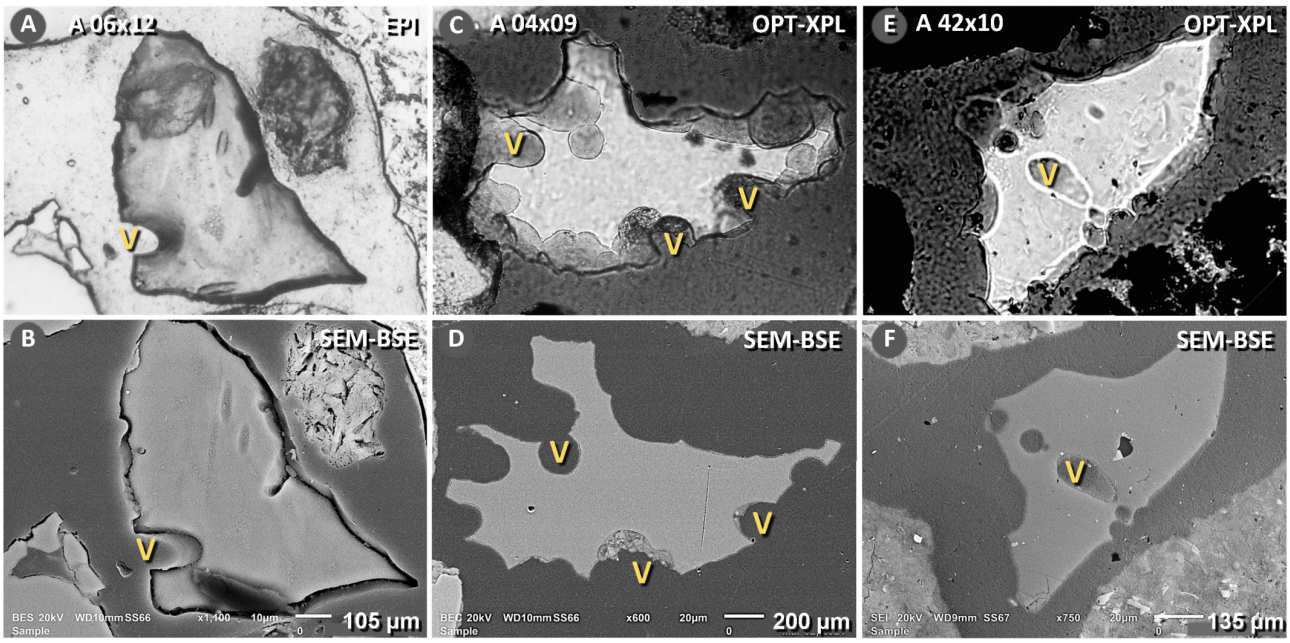


Figure 15: Additional melted vesicular feldspar grains. All grains are isotropic under crossed polars without their characteristically visible lamellae or the distinctive extinction of twinning typical of feldspar. "V" marks vesicles in all samples. Composition: sodic feldspar (albite), averaging ~11 wt% Na, 14 wt% Al, 38 wt% Si, and 37 wt% O. These grains are ~10% depleted in oxygen compared to the stoichiometric values for albite, consistent with grains having been exposed to high temperatures that partially dissociated the feldspar and destroyed the typically visible cleavage. A)-B), C)-D), and E)-F) Epi-illuminated photomicrographs and SEM-BSE images, respectively, of vesicular melted feldspar grains.

airburst phenomena. This improved understanding advances our knowledge of near-Earth object hazards.

Tunguska is widely accepted as a large, low-altitude airburst or cluster of airbursts. Our evidence suggests that this airburst released high-velocity, high-energy fragments that struck Earth's surface, formed small impact craters near ground zero, melted surficial sediments, and produced shock-fractured quartz.

Future research directions include expanding the Tunguska sample set and comparing findings with other potential airburst sites. Additional modeling studies incorporating these new data could refine our understanding of the Tunguska event's dynamics and improve risk assessments for future near-Earth object encounters. This work not only illuminates a historic event but also provides crucial insights for predicting and mitigating similar future events.

Materials and methods

Additional details are provided in the Supporting Information https://zenodo.org/records/14727706.

Sample collection

The Tung3 samples were collected in 2008 by Dallas Abbott and Alexei Kiselev from a marsh near Kulik's cabin in the Tunguska epicenter region. This centennial-year expedition sought direct physical evidence of the extreme conditions generated during the 1908 explosion, building on previous site studies [2, 21]. The July 2, 2008 sampling site was in a circular bog ('boleta') characterized by two concentric crater-like raised rims near the epicenter. Historical maps show this feature as a lake, and it remains visible in current Google Earth imagery (Figure 1). The Tung3 sample was collected from one of six holes excavated by Aleksei Kiselev on the bog's raised rim (60.90506°N, 101.95866°E). Collection occurred at the thawed soil/permafrost boundary, approximately 30 centimeters below the surface, where ice was consistently present in all holes.

The site's stratigraphy revealed two distinct black layers, interpreted as charcoal deposits from forest fires, including the Tunguska airburst, overlying reddish soil. Notable among the findings were 'rock-like' materials with hardened outer rims and soft interiors, potentially representing soil subjected to extreme heating during the event. This sampling strategy targeted materials likely to preserve evidence of the extreme conditions generated during the 1908 explosion, particularly in locations showing signs of impact-related alteration.

Sample preparation and analysis

A 25-gram aliquot from the Tung3 sample underwent sonication and sieving to isolate sedimentary grains, including magnetic and glassy microspherules, carbon spherules, melted feldspar, and shocked/melted quartz. As detailed in the following sections, multiple analytical techniques were employed to examine the morphologies, compositions, and internal structures of these selected grains.

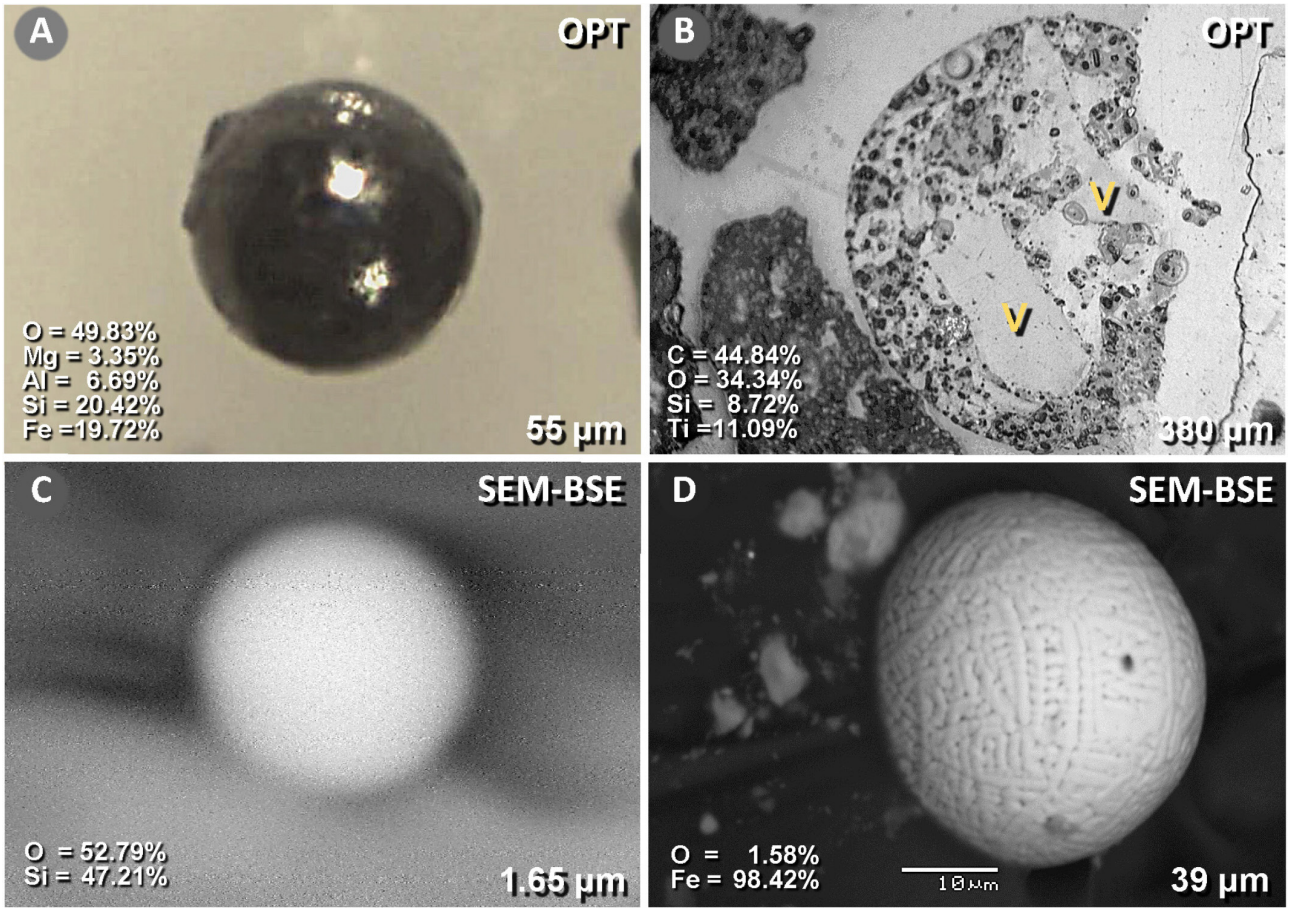


Figure 16: **Tunguska microspherules from near ground zero**. A) Photomicrograph of a 55-µm-diameter Mg-Al-Si-Fe microspherule with a melting point of ~1300°C. B) Epi-illuminated photomicrograph of a sectioned 380-µm-diameter transparent microspherule composed of unusual C-Si-Ti glass with a melting point of ~1300°C. "V" labels indicate large vesicles within the spherule due to outgassing. C) SEM BSE image of a 1.65-µm-diameter melted microspherule with a stoichiometric oxygen/silicon ratio of 53/47 wt%. The melting point of SiO_2 is ~1710°C. D) SEM BSE image of a 39-µm-diameter, dendritic microspherule composed chiefly of native iron (98.42 wt% Fe). All microspherules were extracted from the Tung3 sample and collected at the thawed soil/permafrost contact approximately 30 cm below the surface on the raised crater-like rim of a circular bog near the Tunguska event epicenter.

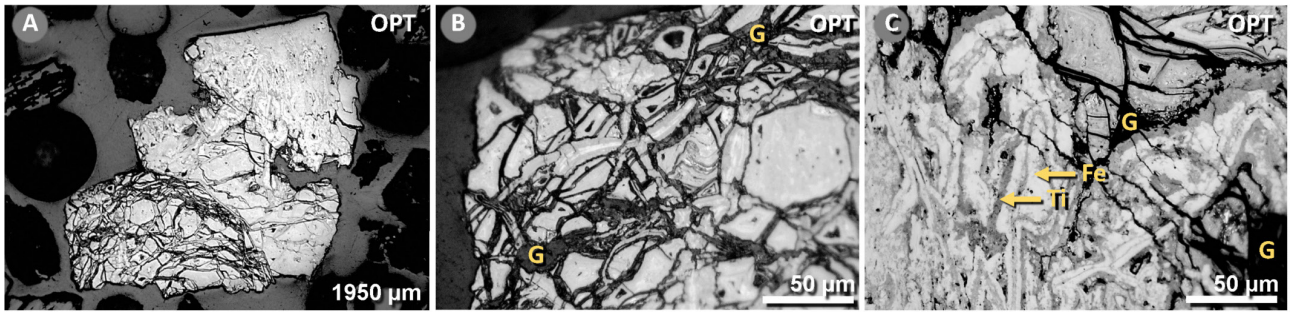


Figure 17: **Partially melted titanomagnetite grain.** A-C) Epi-illuminated photomicrographs of a single (1950-µm-diameter) titanomagnetite grain ($Fe^{2+}(Fe^{3+}, Ti)_2O_4$). A) The lower left of the grain displays evidence of partial melting at ~1625°C, the melting point of titanomagnetite. B) Close-up of the lower left of grain in panel A. Dark areas labeled "G" represent intrusive aluminosilicate material with a melting point of ~1300°C. The intrusions were isotropic under crossed polars, indicative of being amorphous. C) Close-up of the middle right part of the grain in panel A. The Ti (left arrow) has dissociated from the Fe (right arrow).

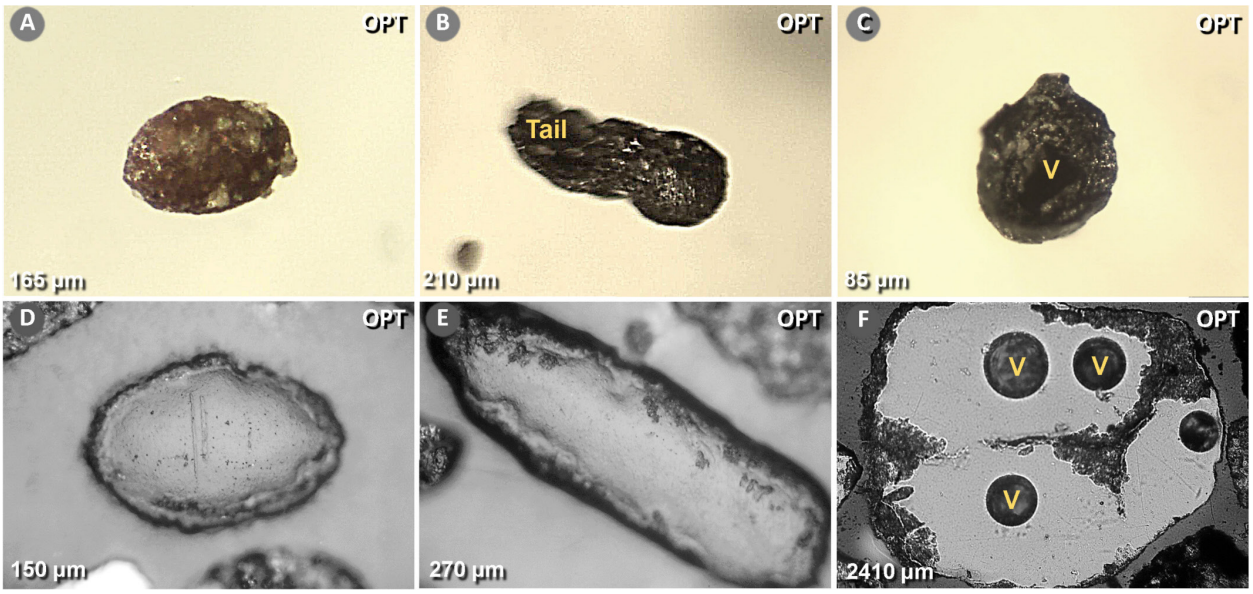


Figure 18: A-C, Photomicrographs of Carbon Spherules. Average composition: >98% C; size range: 86-210 μm.: A) Amber-colored; B) tailed spherule that probably cooled while airborne; C) carbon spherule with large central vesicle, marked as "V," visible with a binocular microscope but unclear in a 2D image. D) Epi-illuminated photomicrograph of a thin-sectioned, 150-μm-long melted carbon particle. E) Epi-illuminated photomicrograph of a thin-sectioned, 2700-μm-long glass-like carbon particle. F) Optical photomicrograph of a thin-sectioned, vesicular, 2410-μm-wide glass-like carbon particle.

Table 1: Summary of materials identified.

Material	Observation	Temperature indication	Pressure indication
FeO microspherules	55-μm and 39-μm wide spherules	>1377°C	-
Aluminosilicate glass microspherules	380-μm wide spherule with vesicles	>1300°C	-
Silicious (quartz) microspherules	1.65-μm wide melted spherule	>1710°C	-
Carbon spherules	85-210 μm wide, various morphologies	800-1200°C	-
Titanomagnetite	Partially melted 1950-μm grain	>1625°C	-
Shocked feldspar	Vesicular melted grains, oxygen-depleted	>1100°C	-
Shocked quartz	Glass-filled fractures, shock lamellae	>1710°C	~>2 GPa
Shocked quartz	Dauphiné twinning, lattice distortions	>1710°C	~>2 GPa

The temperatures listed are for equilibrium conditions that are unlikely to occur in an airburst/impact event. Under laboratory conditions, flux-mediated non-equilibrium temperatures are estimated to be ~200°C lower [40].

Table 2: Airburst parameters used to model the Tunguska event.

Tunguska event
Asteroid diameter = 60 m
Density = 2700 kg/m^3 = 2.7 g/cm^3
Impactor velocity = 20 km/s
Entry angle = 45°
Target density = 2500 kg/m^3
Energy, Mt, atmosphere = 14.6 Mt
Airburst energy = 13.4 Mt
Initial breakup = 59.9 km
Airburst altitude = 5.74 km
Residual velocity = 5.73 km/s
Overpressure = 260000 Pa = 0.00026 GPa
Wind velocity = 211 m/s
Impact recurrence = 1300 years
Large fragments may strike the surface.

Data from Marcus et al. [44] and the Earth Impact Effects Program developed by Marcus et al. [41].

Optical microscopy

Initial examination of selected sedimentary grains was done with optical microscopy at magnifications from 4× to 100×, identifying microspherules, carbon spherules, and mineral grains. Transmitted and reflected light (epi-illumination) microscopy was used to study particle characteristics following standard petrographic techniques [126].

Scanning electron microscopy (SEM)

SEM images were acquired using a JEOL-6000 SEM system in low-vacuum mode and a ThermoFisher Apreo 2 SEM microscope with a cathodoluminescence (CL) detector to obtain high-resolution images of particles and their surfaces and to perform elemental analyses. A backscattered electron (BSE) detector was also used to determine composition. Energy-dispersive X-ray spectroscopy (EDS) was employed to determine elemental compositions and ratios of grains,

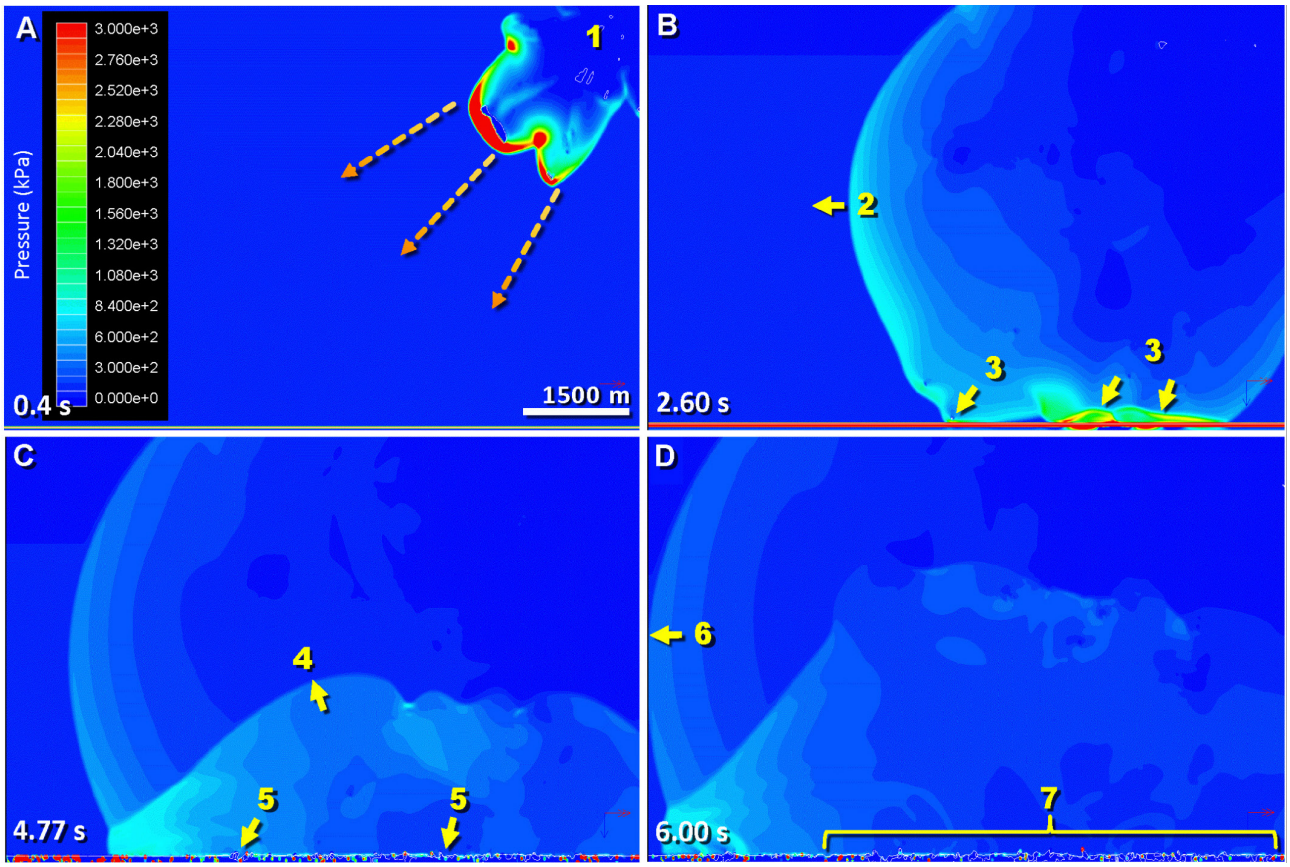


Figure 19: Hydrocode model of the Tunguska airburst. Pressure representation. The model's assumptions from Marcus et al. [41, 44] are that a 60-m-wide stony asteroid entered Earth's atmosphere at 20 km/s with an entry angle of 45° (yellow dashed line). Friction caused it to break up in an airburst at an altitude of 5.74 km with an energy of 14.6 megatons and temperatures >4000 K. These are within the range of accepted conditions cited by multiple studies of the Tunguska event [65]. A) At 0.4 s, the plume of hot vapor and small fragments (#1) was ~2 km wide. B) At 2.6 s, the plume was ~7 km wide (#2) and continued to expand. The shockwave carrying small bolide fragments struck Earth's surface (#3) at ~2.3 km/s. The fragments generated pressures >2 GPa, sufficient to produce shock metamorphism in quartz. C) By 4.77 s, the plume had rebounded off Earth's surface in an upward-moving reflection wave (#4), as additional bolide fragments continued to strike the Earth at >2 km/s (#5), creating more small craters. D) After 6.00 s, the plume's shockwave was >10 km wide (#6), and bolide fragments damaged Earth's surface across ~6 km (#7). Images created with Autodyn-2D, versions 2023 R1 and 2023 R1 Student (Ansys, Inc.).

particularly for microspherules and melted mineral grains, following the methods described by Reed [127].

Transmission and scanning transmission electron microscopy (STEM)

TEM and STEM analyses were performed on selected quartz grains to examine their internal structures at high resolution. The focused ion beam technique was used to prepare thin foils from specific areas of interest within the quartz grains, following procedures outlined by Giannuzzi and Stevie [128]. High-resolution TEM (HRTEM) and dark-field imaging were employed to study lattice structures and identify amorphous regions using an FEI 80-300 Titan scanning/transmission electron microscope.

Electron backscatter diffraction (EBSD)

EBSD analysis was conducted on quartz grains to determine their crystalline structure and orientation using a Teneo system detector. This technique provided information on lattice distortions, misorientations, and recrystallization patterns within the grains, following the methods described by Giannuzzi and Stevie [129].

Cathodoluminescence (CL)

CL imaging was used to examine the internal structures of quartz grains, particularly to identify areas of recrystallization and distinguish between the grains' crystalline and amorphous regions. The analysis was performed using a Monarc CL Detector (Gatan; Pleasanton, CA), following procedures outlined by Götze et al. [130].

Shocked quartz

Quartz grains from the Tunguska airburst layer underwent sequential analytical procedures. Two microscope slides, each containing ~2000 quartz grains, were thin-sectioned, polished, and etched with hydrofluoric acid (HF). Analysis proceeded

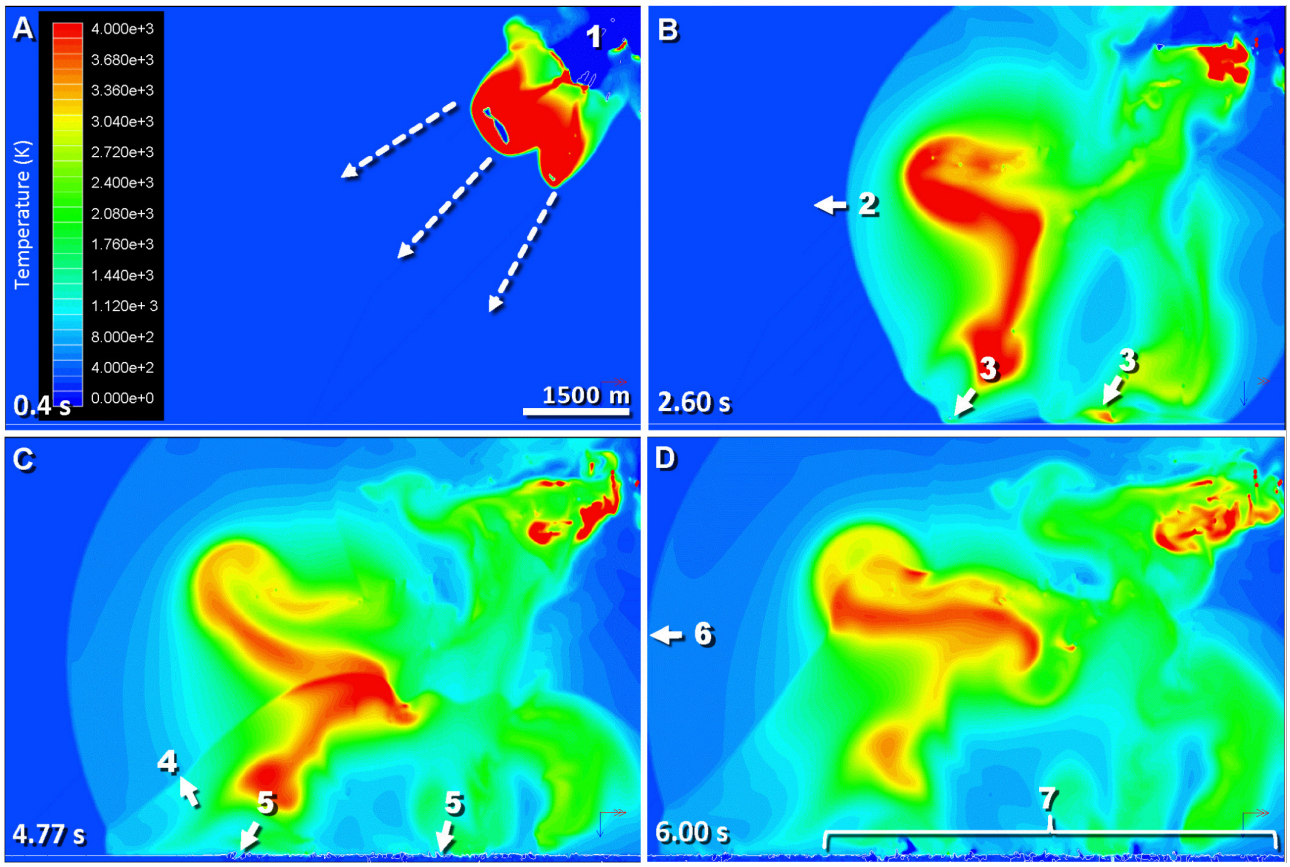


Figure 20: Hydrocode model of the Tunguska airburst. Temperature representation. A) At 0.4 s, the plume of hot vapor and small fragments was ~2 km wide. B) At 2.6 s, the plume was ~7 km wide (#2). The shockwave containing small bolide fragments struck Earth's surface (#3) at ~2.3 km/s. The impacting fragments generated highly transient temperatures of >4000 K, sufficient to partially melt quartz and feldspar. However, most of the ground surface was exposed to temperatures of <1200 K below the melting point of feldspar. C) By 4.77 s, the plume had rebounded off Earth's surface in a reflection wave (#4), as additional bolide fragments continued to strike the Earth at >2 km/s (#5), creating more small craters. D) After 6.00 s, the plume's shockwave was >10 km wide (#6), and bolide fragments damaged Earth's surface across ~6 km (#7). Images created with Autodyn-2D, versions 2023 R1 and 2023 R1 Student (Ansys, Inc.).

through multiple techniques: optical microscopy with crossed polars and epi-illumination identified potential lamellae; SEM-EDS confirmed quartz composition and imaged visible lamellae; cathodoluminescence (CL) investigated luminescence; EBSD identified lamellae with damaged lattice; and universal stage measurements recorded lamellae azimuth and inclination [107, 109, 131]. Finally, the crystallographic axes were plotted with the ANIE indexing program [36] and compared to commonly observed lamellae for quartz [37].

Data analysis

Quantitative analyses of elemental compositions were performed using standardized EDS procedures [132]. Crystallographic data from EBSD were processed using a technique called "PRIAS," an acronym for "Pattern Region of Interest Analysis System," to generate orientation maps and pole figures. Using ThermoFisher Noran System 7 software, image analyses were conducted to measure particle sizes and quantify structural features observed in the SEM, TEM, and CL images.

Temperature estimations

Melting temperatures for various materials were estimated based on known equilibrium melting points of minerals and compounds identified within the samples [133, 134]. These were used to assess the minimum temperatures reached during the Tunguska event. Non-equilibrium temperatures are typically lower by 200-300°C [40].

This comprehensive suite of analytical techniques allowed for detailed characterization of the microscopic particles and minerals found near the Tunguska epicenter, thus providing insights into the extreme conditions generated during the 1908 Tunguska impact event.

Supplementary information includes details on the methods used in this paper. See https://zenodo.org/records/14727706.

Author's contributions

G.K. and A.W. conceived and directed the project. G.K., C.R.M., A.W., M.A.L., M.T., L.S., and R.K. wrote the manuscript. G.K., M.T., L.S., R.K., M.A.L., C.R.M., J.P.K., V.A., T.W., K.L., J.J.R., V.B., B.vanD. contributed data and technical analysis. J.P.P., R.P., D.A., T.M.E, M.V., D.B.L. Jr., Y.R., A.R., R.H., M.M., A.K., and A.W. All authors reviewed and approved the manuscript.

Potential conflicts of interest

The Comet Research Group (CRG), a 501(C) (3) nonprofit charitable organization, provided research funding. J.P.K., M.A.L., C.R.M., and A.W. volunteer their time as co-founders and directors of CRG. No co-author receives a salary, compensation, stock, or any other financial benefit from CRG, except for tax deductions for CRG donations by co-authors A.W., T.W., and M.A.L. All co-authors may receive reimbursements from their respective organizations for attending symposia on the research presented in this paper. A.W. is a co-author of a book about impact events; he donates all proceeds to the nonprofit Comet Research Group. The authors declare no other competing interests.

Funding

G.K.'s work was partially supported by the Czech Science Foundation (Grant 23-06075S). The study was further funded by the Comet Research Group (CRG), the University of California Santa Barbara, the University of South Carolina (USC), and the South Carolina Institute for Archaeology and Anthropology (SCIAA), primarily through a generous grant from Eugene Jhong.

Data availability

All study findings are supported by data within the manuscript and supplementary information files. Bulk and sediment samples were fully expended during analysis.

References

[1] Vasilyev, N.V. The Tunguska Meteorite Problem Today. *Planet. Space Sci.* **1998**, *46*, 129–150; DOI:10.1016/S0032.0633(97)00145.1.

[2] Longo, G.; Serra, R.; Cecchini, S.; Galli, M. Search for Microremnants of the Tunguska Cosmic Body. *Planet. Space Sci.* **1994**, *42*, 163–177; DOI:10.1016/0032.0633(94)90028.0.

[3] Chyba, C.F.; Thomas, P.J.; Zahnle, K.J. The 1908 Tunguska Explosion: Atmospheric Disruption of a Stony Asteroid. *Nature* **1993**, *361*, 40–44; DOI:10.1038/361040a0.

[4] Sekanina, Z. Evidence for Asteroidal Origin of the Tunguska Object. *Planet. Space Sci.* **1998**, *46*, 191–204; DOI:10.1016/S0032.0633(96)00154.7.

[5] Bronshten, V. Nature and Destruction of the Tunguska Cosmical Body. *Planet. Space Sci.* **2000**, *48*, 855–870; DOI:10.1016/S0032.0633(00)00028.3.

[6] Artemieva, N.A.; Shuvalov, V.V. From Tunguska to Chelyabinsk via Jupiter. *Annu. Rev. Earth Planet. Sci.* **2016**, *44*, 37–56; DOI:10.1146/annurev.earth.060115.012218.

[7] Gasperini, L.; Alvisi, F.; Biasini, G.; Bonatti, E.; Longo, G.; Pipan, M.; Ravaioli, M.; Serra, R. A Possible Impact Crater for the 1908 Tunguska Event. *Terra Nova* **2007**, *19*, 245–251; DOI:10.1111/j.1365.3121.2007.00742.x.

[8] Kulik, L. Data on the Tunguska Meteorite up to 1939. *DAS SSSR* **1939**, 520–524.

[9] Krinov, E.L. Giant Meteorites. *Oxford* **1966**.

[10] Longo, G.; Di Martino, M.; Andreev, G.; Anfinogenov, J.; Budaeva, L.; Kovrigin, E. A New Unified Catalogue and a New Map of the 1908 Tree Fall in the Site of the Tunguska Cosmic Body Explosion. *Asteroid-Comet Hazard* **2005**, *2005*, 222–225.

[11] Boslough, M. Computational Modeling of Low-Altitude Airbursts. In AGU Fall Meeting Abstracts, #U21E-03, 2007.

[12] Boslough, M.B.; Crawford, D.A. Low-Altitude Airbursts and the Impact Threat-Final LDRD Report. Sandia National Lab. (SNL-NM), Albuquerque, NM, USA, 2007.

[13] Moore, A.M.T.; Kennett, J.P.; LeCompte, M.A.; Moore, C.R.; Li, Y.-Q.; Kletetschka, G.; Langworthy, K.; Razink, J.J.; Brogden, V.; van Devener, B.; et al. Abu Hureyra, Syria, Part 1: Shock-Fractured Quartz Grains Support 12,800-year-Old Cosmic Airburst at the Younger Dryas Onset. *Airburst. Crater. Imp.* **2023**, *1*, 1–28; DOI:10.14293/ACI.2023.0003.

[14] Moore, A.M.T.; Kennett, J.P.; Napier, W.M.; Bunch, T.E.; Weaver, J.C.; LeCompte, M.A.; Victor Adedeji, A.; Kletetschka, G.; Hermes, R.E.; et al. Abu Hureyra, Syria, Part 2: Additional Evidence Supporting the Catastrophic Destruction of this Prehistoric Village by a Cosmic Airburst ~12,800 years Ago. *Airburst. Crater. Imp.* **2023**, *1*, 1–36; DOI:10.14293/ACI.2023.0002.

[15] Moore, A.M.T.; Kennett, J.P.; Napier, W.M.; Bunch, T.E.; Weaver, J.C.; LeCompte, M.A.; Adedeji, A.V.; Kletetschka, G.; Hermes, R.E.; Wittke, J.H.; et al. Abu Hureyra, Syria, Part 2: Additional Evidence Supporting the Catastrophic Destruction of this Prehistoric Village by a Cosmic Airburst ~12,800 years Ago. *Supplementary Data* **2023**, *1*, 1–25.

[16] Moore, A.M.T.; Kennett, J.P.; Napier, W.M.; LeCompte, M.A.; Moore, C.R.; West, A. Abu Hureyra, Syria, Part 3: Comet Airbursts Triggered Major Climate Change 12,800 years Ago that Initiated the Transition to Agriculture. *Airburst. Crater. Imp.* **2023**, *1*, 1–24; DOI:10.14293/ACI.2023.0004.

[17] Silvia, P.J.; Collins, S.; LeCompte, M.A.; Costa, L.; Howard, G.A.; Kennett, J.P.; Moore, C.R.; Kletetschka, G.; Victor Adedeji, A.; Hermes, R.E.; et al. Modeling how a Powerful Airburst Destroyed Tall el-Hammam, a Middle Bronze Age City near the Dead Sea. *Airburst. Crater. Imp.* **2024**, *2*, 1–52; DOI:10.14293/ACI.2024.0005.

[18] Bunch, T.E.; LeCompte, M.A.; Victor Adedeji, A.; Wittke, J.H.; David Burleigh, T.; Hermes, R.E.; Mooney, C.; Batchelor, D.; Wolbach, W.S.; Kathan, J.; et al. A Tunguska Sized Airburst Destroyed Tall el-Hammam a Middle Bronze Age City in the Jordan Valley near the Dead Sea. *Sci. Rep.* **2021**, *11*, 1–64; DOI:10.1038/s41598.021.97778.3.

[19] Kletetschka, G.; Procházka, V.; Fantucci, R.; Trojek, T. Survival Response of Larix Sibirica to the Tunguska Explosion. *Tree-Ring Res.* **2017**, *73*, 75–90; DOI:10.3959/1536.1098.73.2.75.

[20] Vaganov, E.A.; Hughes, M.K.; Silkin, P.P.; Nesvetailo, V.D. The Tunguska Event in 1908: Evidence from Tree-Ring Anatomy. *Astrobiology* **2004**, *4*, 391–399; DOI:10.1089/ast.2004.4.391.

[21] Kolesnikov, E.; Kolesnikova, N.; Boettger, T. Isotopic Anomaly in Peat Nitrogen is a Probable Trace of Acid Rains Caused by

1908 Tunguska Bolide. *Planet. Space Sci.* **1998**, *46*, 163–167; DOI:10.1016/S0032.0633(97)00190.6.

[22] Longo, G. The Tunguska Event. In *Comet/Asteroid Impacts and Human Society: An Interdisciplinary Approach*, Springer: Berlin/Heidelberg, 2007; pp. 303–330; DOI:10.1007/978.3.540.32711.0_18.

[23] Kletetschka, G.; Kavková, R.; Navátil, T.; Takác, M.; Prach, J.; Vondrák, D.; Stuchlik, E.; Štorc, R.; Švecová, E.; Horická, Z.; et al. New Implications for Tunguska Explosion Based on Magnetic, Dendrological, and Lacustrine Records. In *82nd Annual Meeting of The Meteoritical Society*, 2019; pp. 6506.

[24] Kavková, R.; Vondrák, D.; Chattová, B.; Svecova, E.; Takac, M.; Golias, V.; Štorc, R.; Stanghellini, C.; Kletetschka, G. Suzdalevo Lake (Central Siberia, Russia)—A Tunguska Event-Related Impact Crater? *Front. Earth Sci.* **2022**, *10*, 569; DOI:10.3389/feart.2022.777631.

[25] Fantucci, R.; Serra, R.; Kletetschka, G.; Di Martino, M. The Tunguska Event and Cheko Lake Origin: Dendrochronological Analysis-Corrigendum. *Int. J. Astrobiol.* **2016**, *15*, 33; DOI:10.1017/S1473550415000403.

[26] Kletetschka, G. Magnetic Signatures Recorded in Rocks and Trees Located Inside the Tunguska Blast 100 years Ago, Implications for Mirror Matter, Comet, and Kimberlitic Pipe Explosion Hypotheses. In *AGU Fall Meeting Abstracts*, 2008; pp. GP21C-0787.

[27] Fantucci, R.; Serra, R.; Kletetschka, G. The Tunguska Event and Cheko Lake Origin: Dendrochronological Analysis. *Int. J. Astrobiol.* **2015**, *14*, 345–357; DOI:10.1017/S1473550414000445.

[28] Farinella, P.; Foschini, L.; Froeschlé, Ch.; Gonczi, R.; Jopek, T.J.; Longo, G.; Michel, P. Probable Asteroidal Origin of the Tunguska Cosmic Body. *Astronomy & Astrophysics* **2001**, *377*, 1081–1097.

[29] Vannucchi, P.; Morgan, J.P.; Della Lunga, D.; Andronicos, C.L.; Morgan, W.J. Direct Evidence of Ancient Shock Metamorphism at the Site of the 1908 Tunguska Event. *Earth Planet. Sci. Lett.* **2015**, *409*, 168–174; DOI:10.1016/j.epsl.2014.11.001.

[30] Hryanina, L. The Bouquet of the Meteorite Craters in the Epicentre of Tunguska Impact 1908 Year. In *Lunar and Planetary Science Conference*, 1999; pp. 1186.

[31] Trepmann, C.A.; Dellefant, F.; Kaliwoda, M.; Hess, K.-U.; Schmahl, W.W.; Hölzl, S. Quartz and Cristobalite Ballen in Impact Melt Rocks from the Ries Impact Structure, Germany, Formed by Dehydration of Shock-Generated Amorphous Phases. *Meteorit. Planet. Sci.* **2020**, *55*, 2360–2374; DOI:10.1111/maps.13590.

[32] Hamers, M.; Drury, M. Scanning Electron Microscope-Cathodoluminescence (SEM-CL) Imaging of Planar Deformation Features and Tectonic Deformation Lamellae in Quartz. *Meteorit. Planet. Sci.* **2011**, *46*, 1814–1831; DOI:10.1111/j.1945.5100.2011.01295.x.

[33] Hamers, M.; Pennock, G.; Drury, M. Scanning Electron Microscope Cathodoluminescence Imaging of Subgrain Boundaries, Twins and Planar Deformation Features in Quartz. *Phys. Chem. Miner.* **2017**, *44*, 263–275; DOI:10.1007/s00269.016.0858.x.

[34] Hamers, M.F. *Identifying Shock Microstructures in Quartz from Terrestrial Impacts: New Scanning Electron Microscopy Methods*, UU Department of Earth Sciences, 2013.

[35] Hamers, M.F.; Pennock, G.M.; Herwegh, M.; Drury, M.R. Distinction between Amorphous and Healed Planar Deformation Features in Shocked Quartz using Composite Color Scanning Electron Microscope Cathodoluminescence (SEM-CL) Imaging. *Meteorit. Planet. Sci.* **2016**, *51*, 1914–1931; DOI:10.1111/maps.12711.

[36] Huber, M.S.; Ferriere, L.; Losiak, A.; Koeberl, C. ANIE: A Mathematical Algorithm for Automated Indexing of Planar Deformation Features in Quartz Grains. *Meteorit. Planet. Sci.* **2011**, *46*, 1418–1424; DOI:10.1111/j.1945.5100.2011.01234.x.

[37] French, B.M. *Traces of Catastrophe: A Handbook of Shock-Metamorphic Effects in Terrestrial Meteorite Impact Structures*, Lunar and Planetary Institute, 1998; pp. 120.

[38] Badyukov, D.; Ivanov, A.; Raitala, J.; Khisina, N. Spherules from the Tunguska Event Site: Could they Originate from the Tunguska Cosmic Body? *Geochem. Int.* **2011**, *49*, 641–653; DOI:10.1134/S0016702911070032.

[39] Florenskiy, K. Preliminary Results from the 1961 Combined Tunguska Meteorite Expedition. *Meteoritica* **1965**, *XXIII*, 3–37.

[40] Moore, A.M.T.; Kennett, J.P.; Napier, W.M.; Bunch, T.E.; Weaver, J.C.; LeCompte, M.; Victor Adedeji, A.; Hackley, P.; Kletetschka, G.; Hermes, R.E.; et al. Evidence of Cosmic Impact at Abu Hureyra, Syria at the Younger Dryas Onset (~12.8 ka): High-Temperature Melting at >2200°C. *Sci. Rep.* **2020**, *10*, 4185; DOI:10.1038/s41598.020.60867.w.

[41] Marcus, R.; Melosh, H.J.; Collins, G.S. *Earth Impact Effects Program*. Available online: https://impact.ese.ic.ac.uk/ImpactEarth/ImpactEffects/ (2004).

[42] Collins, G.S.; Lynch, E.; McAdam, R.; Davison, T.M. A Numerical Assessment of Simple Airblast Models of Impact Airbursts. *Meteorit. Planet. Sci.* **2017**, *52*, 1542–1560; DOI:10.1111/maps.12873.

[43] Collins, G.S.; Melosh, H.J.; Marcus, R. Earth Impact Effects Program: A Web-Based Computer Program for Calculating the Regional Environmental Consequences of a Meteoroid Impact on Earth. *Meteorit. Planet. Sci.* **2005**, *40*, 817–840; DOI:10.1111/j.1945.5100.2005.tb00157.x.

[44] Marcus, R.; Melosh, H.J.; Collins, G.S. *Earth Impact Effects Program, Examples*. Available online: https://impact.ese.ic.ac.uk/ImpactEarth/ImpactEffects/examples.html (2004).

[45] Collins, G.S.; Melosh, H.J.; Osinski, G.R. The Impact-Cratering Process. *Elements* **2012**, *8*, 25–30; DOI:10.2113/gselements.8.1.25.

[46] Mathias, D.L.; Wheeler, L.F.; Dotson, J.L. A Probabilistic Asteroid Impact Risk Model: Assessment of Sub-300 m Impacts. *Icarus* **2017**, *289*, 106–119; DOI:10.1016/j.icarus.2017.02.009.

[47] Muthini, J.; Okeng'o, G.O. Modelling the Dynamics of Potentially Dangerous Large-Earth Impactors. *arXiv preprint arXiv:2107.05988*, **2021**.

[48] Osinski, G.R.; Grieve, R.A.F.; Ferrière, L.; Losiak, A.; Pickersgill, A.E.; Cavosie, A.J.; Hibbard, S.M.; Hill, P.J.A.; Bermudez, J.J.; Marion, C.L.; et al. Impact Earth: A Review of the Terrestrial Impact Record. *Earth Sci. Rev.* **2022**, *232*, 104112; DOI:10.1016/j.earscirev.2022.104112.

[49] Robertson, D.K.; Mathias, D.L. Hydrocode Simulations of Asteroid Airbursts and Constraints for Tunguska. *Icarus* **2019**, *327*, 36–47; DOI:10.1016/j.icarus.2018.10.017.

[50] Lv, H.; He, Q.; Chen, X.; Han, P. Numerical Simulation of Impact Crater Formation and Distribution of High-Pressure Polymorphs. *Acta Astronaut.* **2023**, *203*, 169–186; DOI:10.1016/j.actaastro.2022.11.048.

[51] Pierazzo, E.; Artemieva, N.; Asphaug, E.; Baldwin, E.C.; Cazamias, J.; Coker, R.; Collins, G.S.; Crawford, D.A.; Davison, T.; Elbeshausen, D.; et al. Validation of Numerical Codes for Impact and Explosion Cratering: Impacts on Strengthless and Metal Targets. *Meteorit. Planet. Sci.* **2008**, *43*, 1917–1938; DOI:10.1111/j.1945.5100.2008.tb00653.x.

[52] West, A.; Young, M.D.; Costa, L.; Kennett, J.P.; Moore, C.R.; LeCompte, M.A.; Kletetschka, G.; Hermes, R.E. Modeling Airbursts by Comets, Asteroids, and Nuclear Detonations: Shock Metamorphism, Meltglass, and Microspherules. *Airburst. Crater. Imp.* **2024**, *2*, 1–30; DOI:10.14293/ACI.2024.0004.

[53] Baldwin, E.; Milner, D.; Burchell, M.; Crawford, I. Shock Wave Propagation and Damage to the Target in Oceanic Impact Events. In *Bridging the Gap II: Effect of Target Properties on the Impact Cratering Process*, 2007; pp. 13–14.

[54] Baldwin, E.; Vocadlo, L.; Crawford, I. Validation of AUTODYN in Replicating Large-Scale Planetary Impact Events. In *36th Annual Lunar and Planetary Science Conference*, 2005; pp. 1380.

[55] Saito, T.; Kaiho, K.; Abe, A.; Katayama, M.; Takayama, K. Hypervelocity Impact of Asteroid/Comet on the Oceanic Crust of the Earth. *Int. J. Impact Eng.* **2008**, *35*, 1770–1777; DOI:10.1016/j.ijimpeng.2008.07.046.

[56] Saito, T.; Kaiho, K.; Abe, A.; Katayama, M.; Takayama, K. Numerical Simulations of Hypervelocity Impact of Asteroid/Comet on the Earth. *Int. J. Impact Eng.* **2006**, *33*, 713–722; DOI:10.1016/j.ijimpeng.2006.09.012.

[57] Birnbaum, N.K.; Cowler, M.; Hayhurst, C. Numerical Simulation of Impact using AUTODYN. In *Proc. 2nd Int. Impact Sympo.*, Beijing, China, 1996.

[58] Deller, J.; Lowry, S.; Snodgrass, C.; Price, M.; Sierks, H. A New Approach to Modelling Impacts on Rubble Pile Asteroid Simulants. *Mon. Not. R. Astron. Soc.* **2016**, *455*, 3752–3762; DOI:10.1093/mnras/stv2584.

[59] Jones, A.P.; Price, D.G.; DeCarli, P.S.; Price, N.; Clegg, R. Impact Decompression Melting: A Possible Trigger for Impact Induced Volcanism and Mantle Hotspots? In *Impact Markers in the Stratigraphic Record*, Springer: Berlin/Heidelberg, 2003; pp. 91–119; DOI:10.1007/978.3.642.55463.6_4.

[60] Nishizawa, M.; Matsui, Y.; Suda, K.; Saito, T.; Shibuya, T.; Takai, K.; Hasegawa, S.; Yano, H. Experimental Simulations of Hypervelocity Impact Penetration of Asteroids into the Terrestrial Ocean and Benthic Cratering. *J. Geophys. Res.* **2020**, *125*, e2019JE006291; DOI:10.1029/2019JE006291.

[61] Stickle, A.; Barnouin, O.S.; Bruck Syal, M.; Cheng, A.; El Mir, C.; Ernst, C.M.; Michel, P.; Oklay, N.; Owen, M.; Price, M.; et al. Impact Simulation Benchmarking for the Double Asteroid Redirect Test (DART). In *47th Annual Lunar and Planetary Science Conference*, 2016; pp. 2832.

[62] Wie, B.; Barbee, B.W.; Pitz, A.; Kaplinger, B.; Hawkins, M.; Winkler, T.; Premaratne, P.; Vardaxis, G.; Lyzhoft, J.; Zimmerman, B.J. *An Innovative Solution to NASA's NEO Impact Threat Mitigation Grand Challenge and Flight Validation Mission Architecture Development*, 2014.

[63] Caldwell, W.K.; Euser, B.; Plesko, C.S.; Larmat, C.; Lei, Z.; Knight, E.E.; Rougier, E.; Hunter, A. Benchmarking Numerical Methods for Impact and Cratering Applications. *Appl. Sci.* **2021**, *11*, 2504; DOI:10.3390/app11062504.

[64] Birnbaum, N.; Cowler, M.; Itoh, M.; Katayama, M.; Obata, H. AUTODYN-An Interactive Non-Linear Dynamic Analysis Program for Microcomputers through Supercomputers. In *Transactions of the 9th International Conference on Structural Mechanics in Reactor Technology*, 1987; Volume B, pp. 1–4.

[65] Morrison, D. *Tunguska Workshop: Applying Modern Tools to Understand the 1908 Tunguska Impact*, 2018.

[66] De Silva, S.; Sharpton, V. Explosive Volcanism, Shock Metamorphism and the K-T Boundary. In *Global Catastrophes in Earth History: An Interdisciplinary Conference on Impacts, Volcanism, and Mass Mortality*, Lunar and Planetary Institute: Houston, TX, 1988; pp. 38.

[67] de Silva, S.L.; Wolff, J.A.; Sharpton, V.L. Explosive Volcanism and Associated Pressures; Implications for Models of Endogenically Shocked Quartz. In *Global Catastrophes in Earth History*, Geological Society of America (Geological Society Special Publication: Boulder, CO, 1990; pp. 139–145.

[68] Bohor, B.F. Shocked Quartz and more; Impact Signatures in Cretaceous/Tertiary Boundary Clays. In *Global Catastrophes in Earth History; An Interdisciplinary Conference on Impacts, Volcanism, and Mass Mortality*, Sharpton, V.L., Ward, P.D., Eds.; Geological Society of America, 1990.

[69] Houser, L.M.; Ault, A.K.; Newell, D.L.; Evans, J.P.; Shen, F.-A.; Van Devener, B.R. Nanoscale Textural and Chemical Evolution of Silica Fault Mirrors in the Wasatch Fault Damage Zone, Utah, USA. *Geochem. Geophys. Geosyst.* **2021**, *22*, e2020GC009368; DOI:10.1029/2020GC009368.

[70] Janssen, C.; Wirth, R.; Rybacki, E.; Naumann, R.; Kemnitz, H.; Wenk, H.-R.; Dresen, G. Amorphous Material in SAFOD Core Samples (San Andreas Fault): Evidence for Crush-Origin Pseudotachylytes? *Geophys. Res. Lett.* **2010**, *37*; DOI:10.1029/2009GL040993.

[71] Genareau, K.; Wardman, J.B.; Wilson, T.M.; McNutt, S.R.; Izbekov, P. Lightning-Induced Volcanic Spherules. *Geology* **2015**, *43*, 319–322; DOI:10.1130/G36255.1.

[72] Chen, J.; Elmi, C.; Goldsby, D.; Gieré, R. Generation of Shock Lamellae and Melting in Rocks by Lightning-Induced Shock Waves and Electrical Heating. *Geophys. Res. Lett.* **2017**, *44*, 8757–8768; DOI:10.1002/2017GL073843.

[73] Ende, M.; Schorr, S.; Kloess, G.; Franz, A.; Tovar, M. Shocked Quartz in Sahara Fulgurite. *Eur. J.Mineral.* **2012**, *24*, 499–507; DOI:10.1127/0935.1221/2012/0024.2188.

[74] Gieré, R.; Wimmenauer, W.; Müller-Sigmund, H.; Wirth, R.; Lumpkin, G.R.; Smith, K.L. Lightning-Induced Shock Lamellae in Quartz. *Am. Mineral.* **2015**, *100*, 1645–1648; DOI:10.2138/am.2015.5218.

[75] Ferrière, L.; Alwmark, C.; Holm-Alwmark, S.; Leroux, H.; Koeberl, C. Finding, Characterization, and Significance of Shocked Quartz Grains. In *81st Annual Meeting of the Meteoritical Society*, 2018; pp. 6274.

[76] McNutt, S.R.; Davis, C.M. Lightning Associated with the 1992 Eruptions of Crater Peak, Mount Spurr Volcano, Alaska. *J. Volcanol. Geotherm. Res.* **2000**, *102*, 45–65; DOI:10.1016/S0377.0273(00)00181.5.

[77] Bunch, T.E.; Hermes, R.E.; Moore, A.M.; Kennett, D.J.; Weaver, J.C.; Wittke, J.H.; DeCarli, P.S.; Bischoff, J.L.; Hillman, G.C.; Howard, G.A.; et al. Very High-Temperature Impact Melt Products as Evidence for Cosmic Airbursts and Impacts 12,900 Years Ago. *Proc. Natl. Acad. Sci. U. S. A.* **2012**, *109*, E1903–E1912; DOI:10.1073/pnas.1204453109.

[78] Firestone, R.B.; West, A.; Kennett, J.P.; Becker, L.; Bunch, T.E.; Revay, Z.S.; Schultz, P.H.; Belgya, T.; Kennett, D.J.; Erlandson, J.M.; et al. Evidence for an Extraterrestrial Impact 12,900 Years Ago that Contributed to the Megafaunal Extinctions and the Younger Dryas Cooling. *Proc. Natl. Acad. Sci. U. S. A.* **2007**, *104*, 16016–16021; DOI:10.1073/pnas.0706977104.

[79] Abramov, N.B.; Doroshin, I.K.; Klykov, O.I.; Krasavchikov, V.O.; Yashkov, D.V. Some Research Results of the 1908 Tunguska Event Related Fire. In Abstracts of the International Conference "90th Anniversary of the Tunguska Problem", Krasnoyarsk, Russia, June 30–July 2, 1998.

[80] Hermes, R.E.; Wenk, H.-R.; Kennett, J.P.; Bunch, T.E.; Moore, C.R.; LeCompte, M.A.; Kletetschka, G.; Adedeji, A.V.; Langworthy, K.; Razink, J.; et al. Microstructures in Shocked Quartz: Linking Nuclear Airbursts and Meteorite Impacts. *Airburst. Crater. Imp.* **2023**, *1*, 1–40; DOI:10.14293/ACI.2023.0001.

[81] Gladysheva, O.G. The Descent of Pieces of the Tunguska Cosmic Body. *Nat. Sci.* **2013**, *5*; DOI:10.4236/ns.2013.55071.

[82] Carbognani, A.; Di Martino, M.; Stirpe, G. Computation of a Possible Tunguska's Strewn Field. *Icarus* **2024**, *408*, 115845; DOI:10.1016/j.icarus.2023.115845.

[83] Kvasnytsya, V.; Wirth, R.; Dobrzhinetskaya, L.; Matzel, J.; Jacobsen, B. New Evidence of Meteoritic Origin of the Tunguska Cosmic Body. *Planet. Space Sci.* **2013**, *84*, 131–140; DOI:10.1016/j.pss.2013.05.003.

[84] Artemieva, N.; Shuvalov, V. Atmospheric Shock Waves after Impacts of Cosmic Bodies up to 1000 m in Diameter. *Meteorit. Planet. Sci.* **2019**, *54*, 592–608; DOI:10.1111/maps.13229.

[85] Kletetschka, G.; Vyhnanek, J.; Kawasumiova, D.; Nabelek, L.; Petrucha, V. Localization of the Chelyabinsk Meteorite from Magnetic Field Survey and GPS Data. *IEEE Sens. J.* **2015**, *15*, 4875–4881; DOI:10.1109/JSEN.2015.2435252.

[86] Brown, P.G.; Assink, J.D.; Astiz, L.; Blaauw, R.; Boslough, M.B.; Borovička, J.; Brachet, N.; Brown, D.; Campbell-Brown, M.; Ceranna, L.; et al. A 500-Kiloton Airburst Over Chelyabinsk and an Enhanced Hazard from Small Impactors. *Nature* **2013**, *503*, 238–241; DOI:10.1038/nature12741.

[87] Popova, O.P.; Jenniskens, P.; Emel'yanenko, V.; Kartashova, A.; Biryukov, E.; Khaibrakhmanov, S.; Shuvalov, V.; Rybnov, Y.;

Dudorov, A.; Grokhovsky, V.I.; et al. Chelyabinsk Airburst, Damage Assessment, Meteorite Recovery, and Characterization. *Science* **2013**, *342*, 1069–1073; DOI:10.1126/science.1242642.

[88] Kocherov, A.; Korochantsev, A.; Lorenz, C.; Ivanova, M.; Grokhovsky, V. Recovery, Laboratory Preparation and Current State of the Main Mass of the Chelyabinsk Meteorite. In *45th Annual Lunar and Planetary Science Conference*, 2014; pp. 2227.

[89] Brown, P.G.; Hildebrand, A.R.; Zolensky, M.E.; Grady, M.; Clayton, R.N.; Mayeda, T.K.; Tagliaferri, E.; Spalding, R.; MacRae, N.D.; Hoffman, E.L.; et al. The Fall, Recovery, Orbit, and Composition of the Tagish Lake Meteorite: A New Type of Carbonaceous Chondrite. *Science* **2000**, *290*, 320–325; DOI:10.1126/science.290.5490.320.

[90] Brown, P.G.; Revelle, D.O.; Tagliaferri, E.; Hildebrand, A.R. An Entry Model for the Tagish Lake Fireball Using Seismic, Satellite and Infrasound Records. *Meteorit. Planet. Sci.* **2002**, *37*, 661–675; DOI:10.1111/j.1945.5100.2002.tb00846.x.

[91] Bland, P.; Berry, F.; Pillinger, C. Meteorites as Indicators of Paleoclimatic Conditions. In *Abstracts of the Lunar and Planetary Science Conference*, 1995; Volume 26, pp. 129.

[92] Jull, A.; Wlotzka, F.; Bevan, A.; Brown, S.; Donahue, D. 14C Terrestrial Ages of Meteorites from Desert Regions: Algeria and Australia. *Meteoritics* **1993**, *28*, 376.

[93] Bland, P.; Smith, T.B.; Jull, A.J.T.; Berry, F.J.; Bevan, A.W.R.; Cloude, S.; Pillinger, C.T. The Flux of Meteorites to the Earth over the Last 50 000 Years. *Mon. Not. R. Astron. Soc.* **1996**, *283*, 551–565; DOI:10.1093/mnras/283.2.551.

[94] Kieffer, S.W. Shock Metamorphism of the Coconino Sandstone at Meteor Crater, Arizona. *J. Geophys. Res.* **1971**, *76*, 5449–5473; DOI:10.1029/JB076i023p05449.

[95] Kieffer, S.W. From Regolith to Rock by Shock. *Moon* **1975**, *13*, 301–320; DOI:10.1007/BF00567522.

[96] Kieffer, S.W.; Phakey, P.P.; Christie, J.M. Shock Processes in Porous Quartzite: Transmission Electron Microscope Observations and Theory. *Contr. Mineral. Petrol.* **1976**, *59*, 41–93; DOI:10.1007/BF00375110.

[97] Andronikov, A.V.; Rudnickaitė, E.; Lauretta, D.S.; Andronikova, I.E.; Kaminskas, D.; Šinkūnas, P.; Melešytė, M. Geochemical Evidence of the Presence of Volcanic and Meteoritic Materials in Late Pleistocene Lake Sediments of Lithuania. *Quat. Int.* **2015**, *386*, 18–29; DOI:10.1016/j.quaint.2014.10.005.

[98] Spray, J.G. Frictional Melting Processes in Planetary Materials: From Hypervelocity Impact to Earthquakes. *Annu. Rev. Earth Planet. Sci.* **2010**, *38*, 221–254; DOI:10.1146/annurev.earth.031208.100045.

[99] Israde-Alcántara, I.; Bischoff, J.L.; Domínguez-Vázquez, G.; Li, H.C.; DeCarli, P.S.; Bunch, T.E.; Wittke, J.H.; Weaver, J.C.; Firestone, R.B.; West, A.; et al. Evidence from Central Mexico Supporting the Younger Dryas Extraterrestrial Impact Hypothesis. *Proc. Natl. Acad. Sci. U. S. A.* **2012**, *109*, E738–E747; DOI:10.1073/pnas.1110614109.

[100] Scott, A.C.; Pinter, N.; Collinson, M.E.; Hardiman, M.; Anderson, R.S.; Brain, A.P.R.; Smith, S.Y.; Marone, F.; Stampanoni, M. Fungus, not Comet or Catastrophe, Accounts for Carbonaceous Spherules in the Younger Dryas "Impact Layer." *Geophys. Res. Lett.* **2010**, *37*, 1–5; DOI:10.1029/2010GL043345.

[101] Lattard, D.; Engelmann, R.; Kontny, A.; Sauerzapf, U. Curie Temperatures of Synthetic Titanomagnetites in the Fe-Ti-O system. Reassessment of Some Methodological and Crystal Chemical Effects. *J. Geophys. Res.* **2006**, *111*, B12S28; DOI:10.1029/2006JB004591.

[102] Osinski, G.R. Impact Glasses in Fallout Suevites from the Ries Impact Structure, Germany: An Analytical SEM Study. *Meteorit. Planet. Sci.* **2003**, *38*, 1641–1667; DOI:10.1111/j.1945.5100.2003.tb00006.x.

[103] French, B.M.; Koeberl, C. The Convincing Identification of Terrestrial Meteorite Impact Structures: What Works, What Doesn't, and Why. *Earth Sci. Rev.* **2010**, *98*, 123–170; DOI:10.1016/j.earscirev.2009.10.009.

[104] Timms, N.E.; Reddy, S.M.; Healy, D.; Nemchin, A.A.; Grange, M.L.; Pidgeon, R.T.; Hart, R. Resolution of Impact-Related Microstructures in Lunar Zircon: A Shock-Deformation Mechanism Map. *Meteorit. Planet. Sci.* **2012**, *47*, 120–141; DOI:10.1111/j.1945.5100.2011.01316.x.

[105] Christie, J.; Ardell, A. Substructures of Deformation Lamellae in Quartz. *Geology* **1974**, *2*, 405–408; DOI:10.1130/0091-7613(1974)2<405:SODLIQ>2.0.CO;2.

[106] Reimold, W.; Gibson, R. Geology and Evolution of the Vredefort Impact Structure, South Africa. *J Afr. Earth Sci.* **1996**, *23*, 125–162; DOI:10.1016/S0899.5362(96)00059.0.

[107] Langenhorst, F. Shock Metamorphism of Some Minerals: Basic Introduction and Microstructural Observations. *Bull. Czech Geol. Surv.* **2002**, *77*, 265–282.

[108] Shuvalov, V.V.; Trubetskaya, I.A. Aerial Bursts in the Terrestrial Atmosphere. *Sol. Syst. Res.* **2007**, *41*, 220–230; DOI:10.1134/S0038094607030057.

[109] Stöffler, D.; Langenhorst, F. Shock Metamorphism of Quartz in Nature and Experiment: I. Basic Observation and Theory. *Meteoritics* **1994**, *29*, 155–181; DOI:10.1111/j.1945.5100.1994.tb00670.x.

[110] Wasson, J.T. Large Aerial Bursts: An Important Class of Terrestrial Accretionary Events. *Astrobiology* **2003**, *3*, 163–179; DOI:10.1089/153110703321632499.

[111] Ferrière, L.; Koeberl, C.; Reimold, W. U. Characterisation of Ballen Quartz and Cristobalite in Impact Breccias: New Observations and Constraints on Ballen Formation. *Eur. J. Mineral.* **2009**, *21*, 203–217; DOI:10.1127/0935.1221/2009/0021.1898.

[112] Langenhorst, F. Shock Experiments on Pre-Heated α-and β-Quartz: II. X-ray and TEM Investigations. *Earth Planet. Sci. Lett.* **1994**, *128*, 683–698; DOI:10.1016/0012.821X(94)90179.1.

[113] Gault, D.; Quaide, W.; Oberbeck, V.; French, B.; Short, N. *Shock Metamorphism of Natural Materials*, Mono Book Corporation: Baltimore, 1968; pp. 87–99.

[114] Molnár, M.; Švanda, P.; Štaffen, Z.; Rappenglueck, M.; Ernstson, K. Chrudim-Pardubice: Evidence for a Young Meteorite Impact Strewn Field in the Czech Republic. In *48th Annual Lunar and Planetary Science Conference*, 2017; pp. 1920.

[115] Poßekel, J.; Molnár, M.; Ernstson, K. The Proposed Meteorite Impact Event in the Czech Republic: Evidence Strengthened by Investigations with the Digital Terrain Model. *53rd Lunar and Planetary Science Conference* **2022**, *2678*, 1558.

[116] Ernstson, K.; Müller, W.; Gawlik-Wagner, A. The Saarlouis Semi Crater Structure: Notable Insight into the Saarland (Germany) Meteorite Impact Event Achieved, Abstract and Poster #1876. In *49th Lunar and Planetary Science Conference.* Abstract and Poster #1876, 2018.

[117] Ernstson, K.; Mayer, W.; Neumair, A.; Rappenglück, B.; Sudhaus, D. The Chiemgau Crater Strewn Field: Evidence of a Holocene Large Impact Event in Southeast Bavaria, Germany. *J. Sib. Fed.* **2010**, *3*, 72–103.

[118] Ernstson, K.; Sideris, C.; Liritzis, I.; Neumair, A. The Chiemgau Meteorite Impact Signature of the Stöttham Archaeological Site (Southeast Germany). *Mediterr. Archaeol. Archaeom.* **2012**, *12*, 249–259.

[119] Kalenda, P.; Thinová, L.; Tengler, R.; Procházka, V.; Mizera, J.; Martinec, P.; Kletetschka, G.; Trojek, T. Two Impact Craters at Emmerting, Germany: Field Documentation and Geophysics. *J. Geodyn.* **2024**, *2*, 27–44; DOI:10.23939/jgd2024.02.027.

[120] Waldmann, G.; Herten, F.; Hiltl, M.; Ernstson, K. The Enigmatic Niederrhein (Germany) Deposit: Evidence of a Middle-Pleistocene Meteorite Impact Strewn Field. In *49th Annual Lunar and Planetary Science Conference*, 2018; pp. 1610.

[121] Ernstson, K.; Schulz-Hertlein, G.; Ernstson, T.; Poßekel, J. A Probable Holocene Meteorite Impact Crater Strewn Field in Lower Franconia (Germany): Evidence from Digital Terrain Models and Geophysical Surveys (GPR, Electrical Imaging, Geomagnetics). *Poster, Proceedings of the AGU Fall Meeting*, 2022.

[122] Ernstson, K.; Poßekel, J.; Kurtz, J. The Enigmatic Sachsendorf Bay Structure (Oderbruch, Northeast Germany): Evidence of a Pleistocene/Holocene Meteorite Impact Event. In *12th Planetary Crater Consortium Meeting* **2021**, *12*, 2022.

[123] Ahokas, H. *Thirty-Three Previously Unknown Meteoritic Craters of Diameter from 5 to 100 m in Western Kouvola, Finland from a Swarm of Impactors in the Holocene*, Kave, 2023.

[124] Bailey, B.K.; Cohen, AN.; Egan, S.; Lubin, P.; Xu, R.; Boslough, M.; Robertson, D.; Silber, E.; Sagert, I.; Korobkin, O.; Sjoden, G. Asteroid 2023 NT1: A Cautionary Tale. *arXiv preprint arXiv:2310.13112*, 2023.

[125] Cohen, A.N.; Bailey, B.; Lubin, P.; Boslough, M.; Patel, D.; Robertson, D.; Egan, S.; Silber, E.A. NH33C-0812 Asteroid 2023 NT1–A Cautionary Tale. *AGU23*, 2023.

[126] Ness, W. *Introduction to Optical Mineralogy*, 4th ed.; Oxford University Press, 2013.

[127] Reed, S.J.B. *Electron Microprobe Analysis and Scanning Electron Microscopy in Geology*, Cambridge University Press, 2005.

[128] Giannuzzi, L.A.; Stevie, F.A. *Introduction to Focused Ion Beams: Instrumentation, Theory, Techniques and Practice*, Springer Science & Business Media, 2004.

[129] Prior, D.J.; Mariani, E.; Wheeler, J. EBSD in the Earth Sciences: Applications, Common Practice, and Challenges. In *Electron Backscatter Diffraction in Materials Science*, Springer: Boston, MA, 2009; pp. 345–360.

[130] Götze, J.; Plötze, M.; Habermann, D. Origin, Spectral Characteristics and Practical Applications of the Cathodoluminescence (CL) of Quartz – A Reivew. *Mineral Petrol* **2001**, *71*, 225–250; DOI:10.1007/s007100170040.

[131] Voorn, M. *A New Way to Confirm Meteorite Impact Produced Planar Features in Quartz: Combining Universal Stage and Electron Backscatter Diffraction Techniques*, 2010.

[132] Goldstein, J.I.; Newbury, D.E.; Michael, J.R.; Ritchie, N.W.M.; Scott, J.H.J.; Joy, D.C. *Scanning Electron Microscopy and X-Ray Microanalysis*, 4th ed.; Springer, 2018; pp. 550, ISBN: 978-1-4939-6674-5. *Microscopy and Microanalysis* **2018**, **24**, 768–768.

[133] Feininger, T. *An Introduction to the Rock-Forming Minerals*, Mineralogical Association of Canada, 2013.

[134] Deer, W.A.; Howie, R.A.; Zussman, J. *An Introduction to the Rock-Forming Minerals*, Mineralogical Society of Great Britain and Ireland, 2013.